Molecular Therapy
Methods & Clinical Development
Original Article

CRISPR-Directed Therapeutic Correction at the *NCF1* Locus Is Challenged by Frequent Incidence of Chromosomal Deletions

Dominik Wrona,[1] Oleksandr Pastukhov,[1] Robert S. Pritchard,[4] Federica Raimondi,[1] Joëlle Tchinda,[5] Martin Jinek,[4] Ulrich Siler,[1,6] and Janine Reichenbach[1,2,3,6]

[1]Division of Gene and Cell Therapy, Institute for Regenerative Medicine, University of Zurich, 8952 Schlieren-Zurich, Switzerland; [2]Department of Somatic Gene Therapy, University Children's Hospital Zurich, 8032 Zurich, Switzerland; [3]Children's Research Center, University Children's Hospital Zurich, 8032 Zurich, Switzerland; [4]Department of Biochemistry, University of Zurich, 8057 Zurich, Switzerland; [5]Department of Oncology, University Children's Hospital Zurich, 8032 Zurich, Switzerland

Resurrection of non-processed pseudogenes may increase the efficacy of therapeutic gene editing, upon simultaneous targeting of a mutated gene and its highly homologous pseudogenes. To investigate the potency of this approach for clinical gene therapy of human diseases, we corrected a pseudogene-associated disorder, the immunodeficiency p47^{phox}-deficient chronic granulomatous disease (p47^{phox} CGD), using clustered regularly interspaced short palindromic repeats-associated nuclease Cas9 (CRISPR-Cas9) to target mutated neutrophil cytosolic factor 1 (*NCF1*). Being separated by less than two million base pairs, *NCF1* and two pseudogenes are closely co-localized on chromosome 7. In healthy people, a two-nucleotide GT deletion (ΔGT) is present in the *NCF1B* and *NCF1C* pseudogenes only. In the majority of patients with p47^{phox} CGD, the *NCF1* gene is inactivated due to a ΔGT transfer from one of the two non-processed pseudogenes. Here we demonstrate that concurrent targeting and correction of mutated *NCF1* and its pseudogenes results in therapeutic CGD phenotype correction, but also causes potentially harmful chromosomal deletions between the targeted loci in a p47^{phox}-deficient CGD cell line model. Therefore, development of genome-editing-based treatment of pseudogene-related disorders mandates thorough safety examination, as well as technological advances, limiting concurrent induction of multiple double-strand breaks on a single chromosome.

INTRODUCTION

Chronic granulomatous disease (CGD) is characterized by defective respiratory burst,[1] impaired microbicidal activity of phagocytes,[2,3] and resulting life-threatening bacterial and fungal infections. This condition is caused by mutations of genes encoding gp91^{phox}, p22^{phox}, p67^{phox}, p47^{phox}, or p40^{phox} subunits of the phagocytic nicotinamide adenine dinucleotide phosphate (NADPH) oxidase complex. In nearly all patients with p47^{phox} CGD, the disease is caused by a two-nucleotide GT deletion (ΔGT) within exon 2 of the neutrophil cytosolic factor 1 (*NCF1*) gene.[4,5] This ΔGT mutation causes a frameshift and an early translation termination. *NCF1* is accompanied on chromosome 7 by two almost identical non-processed pseudogenes, *NCF1B* and *NCF1C*, which carry the ΔGT mutation also in healthy individuals.[6,7] Although retroviral-based hematopoietic stem cell (HSC) gene therapy has been clinically successful in patients with the X-linked gp91^{phox}-deficient form of CGD,[8,9] autosomal recessive p47^{phox} CGD has not been successfully addressed in gene therapy trials yet. Because more than 97% of patients with p47^{phox} CGD share the same ΔGT mutation, genome-editing-based gene therapy may constitute an attractive alternative to lentiviral gene therapies for this subgroup of patients.

In general, genetic disorders such as p47^{phox} CGD caused by mutation transfer from non-processed pseudogenes are particularly promising targets for genome editing, because parallel gene and pseudogene resurrection via the presence of highly homologous target sites may potentially increase the overall efficiency of the treatment. If the gene and pseudogene are located on the same chromosome, however, editing inducing double-strand breaks (DSBs) may cause chromosomal deletions as a side effect. At least 11 reported genetic disorders are associated with pseudogene-related gene conversion (Table S1),[10,11] making them potentially attractive, but challenging targets for genome editing. In the case of p47^{phox} CGD, the ΔGT mutation may be directly targeted and corrected, leading to conversion of the inactive *NCF1* loci into p47^{phox}-expressing genes. However, for other pseudogene-related disorders, various strategies may be considered, including exon replacement or minigene insertion.[12,13]

As a model representing pseudogene-related genetic disorders, here we study the efficacy and safety of genome editing of p47^{phox}

Received 4 April 2020; accepted 22 April 2020;
https://doi.org/10.1016/j.omtm.2020.04.015.

[6]These authors contributed equally to this work.

Correspondence: Janine Reichenbach, Division of Gene and Cell Therapy, Institute for Regenerative Medicine, University of Zurich, 8952 Schlieren-Zurich, Switzerland.
E-mail: janine.reichenbach@uzh.ch

CGD by clustered regularly interspaced short palindromic repeats-associated nuclease Cas9 (CRISPR-Cas9). Diverse genome-editing systems (CRISPR-Cas9, zinc-finger nucleases [ZFNs], transcription activator-like effector nucleases [TALENs]) have been used preclinically for correction of CGD in cell line models[14–16] and in human HSCs by cDNA delivery to a safe genomic harbor,[17,18] by exon replacement,[12] or by direct mutation targeting.[19,20] Interestingly, ZFN-mediated correction of *NCF1* pseudogenes in induced pluripotent stem cells (iPSCs) resulted in the expression of functional $p47^{phox}$ upon phagocytic differentiation.[19] Whereas these studies focused primarily on the efficacy of CGD correction, we set out to evaluate the safety of ΔGT $p47^{phox}$ CGD correction in a cell line model of $p47^{phox}$ CGD.[21]

RESULTS

Reconstitution of $p47^{phox}$ Expression and NADPH Oxidase Function upon CRISPR-Cas9-Mediated Correction of *NCF1* Gene and Pseudogene Loci

First, the PLB-985 wild type (WT) and the corresponding isogenic $p47^{phox}$ CGD model cell line, PLB-985 *NCF1* ΔGT,[21] were nucleofected with a CRISPR-Cas9 and GFP co-expressing plasmid, along with a corrective single-stranded oligodeoxynucleotide (ssODN) template (Figure 1A). Single-guide RNA (sgRNA) sequences were designed to guide Cas9 to the ΔGT mutation site in mutated *NCF1*, which is also present in *NCF1B* and *NCF1C* pseudogenes (Figure 1B). The on-target correction efficiency in Cas9-expressing cells was determined by PCR-based restriction fragment length polymorphism (RFLP) method (PCR-RFLP) that detects restoration of the BsrGI restriction site upon correction, quantified as GTGT content in genomic DNA derived from edited cells (Figures 1B and 1C).

This analysis demonstrated that the ΔGT mutation within the *NCF1* gene and its pseudogenes can be corrected, and that two out of three tested sgRNAs (sgRNA #1 and #2; Figures 1B and 1C) successfully reconstituted the BsrG1 restriction site (Figure 1B), restoring the normal *NCF1* gene sequence. The efficiencies of *NCF1* gene and pseudogene loci correction corresponded to the GTGT content values observed for clinically healthy ΔGT $p47^{phox}$ CGD carriers.[22] Estimated GTGT content values for CRISPR-Cas9-treated PLB-985 *NCF1* ΔGT bulk cultures were 0.22 ± 0.02 and 0.17 ± 0.02 for sgRNA #1 and #2, respectively, suggesting that on average one *NCF1* gene or one pseudogene locus was corrected in Cas9-expressing cells. Interestingly, CRISPR-Cas9 treatment of PLB-985 WT cells led to an increase of the GTGT content, from 0.39 ± 0.04 (untreated) to 0.70 ± 0.03, indicating the correction of *NCF1B* or *NCF1C* pseudogenes.

High efficacy of CRISPR-Cas9 editing was observed for all tested sgRNAs, as additionally assayed by TIDER (tracking of insertions, deletions, and recombination events by decomposition) method (Figure 1D).[23] Due to the highly homologous *NCF1* gene and pseudogene loci in humans, as well as a naturally present ΔGT in *NCF1* pseudogenes, TIDER analysis of PLB-985 WT cells, performed on PCR co-amplified *NCF1* gene and pseudogene loci, detects the correct *NCF1* gene as "cleaved and corrected." Therefore, the estimated reference cleavage and correction frequencies for the CRISPR-Cas9-untreated wild-type cells were 46.4% ± 1.3% and 41.8% ± 0.7%, respectively. The cleavage efficiency determined for CRISPR-Cas9-treated PLB-985 WT cells was 93.3% ± 1.7%, and the correction efficiency was 63.1% ± 5.6%.

The true cleavage and correction efficacies in PLB-985 WT cells, corresponding to the difference between values detected in CRISPR-Cas9-treated and untreated cells, confirmed the results observed with PCR-RFLP. In CRISPR-Cas9-treated PLB-985 *NCF1* ΔGT bulk cultures, all tested sgRNAs exhibited high levels of cleavage efficiency: 89.8% ± 0.6%, 56.8% ± 4.4%, and 81.9% ± 6.5% for sgRNAs #1, #2, and #3, respectively. Correction of the ΔGT mutation was observed only with sgRNAs #1 and #2, reaching 29.3% ± 0.9% for sgRNA #1 and 18.9% ± 2.0% for sgRNA #2 (Figure 1D), confirming the results of the PCR-RFLP analysis (Figure 1C).

Analysis of $p47^{phox}$ protein expression in CRISPR-Cas9-treated cells (Figure 1E) showed that correction of the *NCF1* pseudogenes in PLB-985 WT cells led to increased $p47^{phox}$ expression. Correction of PLB-985 *NCF1* ΔGT (achieved with sgRNA #1 and #2) restored $p47^{phox}$ protein expression. In addition, the NADPH oxidase function was reconstituted in CRISPR-Cas9-treated PLB-985 *NCF1* ΔGT cells, as measured by nitroblue tetrazolium (NBT) test (Figure 1F). Remarkably, CRISPR-Cas9 treatment of PLB-985 *NCF1* ΔGT cells without corrective template also reconstituted NADPH oxidase function, although in fewer cells. This was not due to alternative splicing, but likely occurred because of the reading frame-restoring indel mutations in *NCF1* (Figure S1).

Simultaneous Editing of Three *NCF1* Gene and Pseudogene Loci Present on Chromosome 7 Leads to Complex Genomic Aberrations

To characterize potential adverse effects of concurrent CRISPR-Cas9 targeting of *NCF1* gene and pseudogene loci, we generated single clones of CRISPR-Cas9-treated (sgRNA #1) PLB-985 *NCF1* ΔGT cells (Figures S2–S6). The sgRNA #1 has been selected for subsequent experiments because it showed the highest specificity in cleaving the ΔGT carrying sequence among tested sgRNAs (Figure S2). The T7 Endonuclease I assay performed on the top predicted off-target sites showed high specificity of sgRNA #1 toward the mutated *NCF1* and *NCF1* pseudogenes (Figure S7A; Table S2). GUIDE sequencing (GUIDE-seq) analysis[24] revealed three off-target sequences, of which one is represented within five distinct genomic locations in the proximity of members of a large multigene family, olfactory receptors (Figure S7B; Table S3).[25] Analysis by single-molecule real-time (SMRT) sequencing[26] of the *NCF1/NCF1B/NCF1C* PCR co-amplification products, surrounding the ΔGT mutation of CRIPSR-Cas9-treated PLB-985 *NCF1* ΔGT individual clones, revealed high frequency of indel mutations at the *NCF1* on-target site, exceeding 90% of reads from non-corrected *NCF1* gene or pseudogene loci (Table S4). Sixty percent of Cas9-expressing clones exhibited corrected reads (Figure S3A). Furthermore, 5 out of 45 tested clones carried a 0.5-kb deletion at the CRISPR-Cas9 cut site that deleted *NCF1* exon 2 (Figure 2A) and affected the results observed by PCR-RFLP

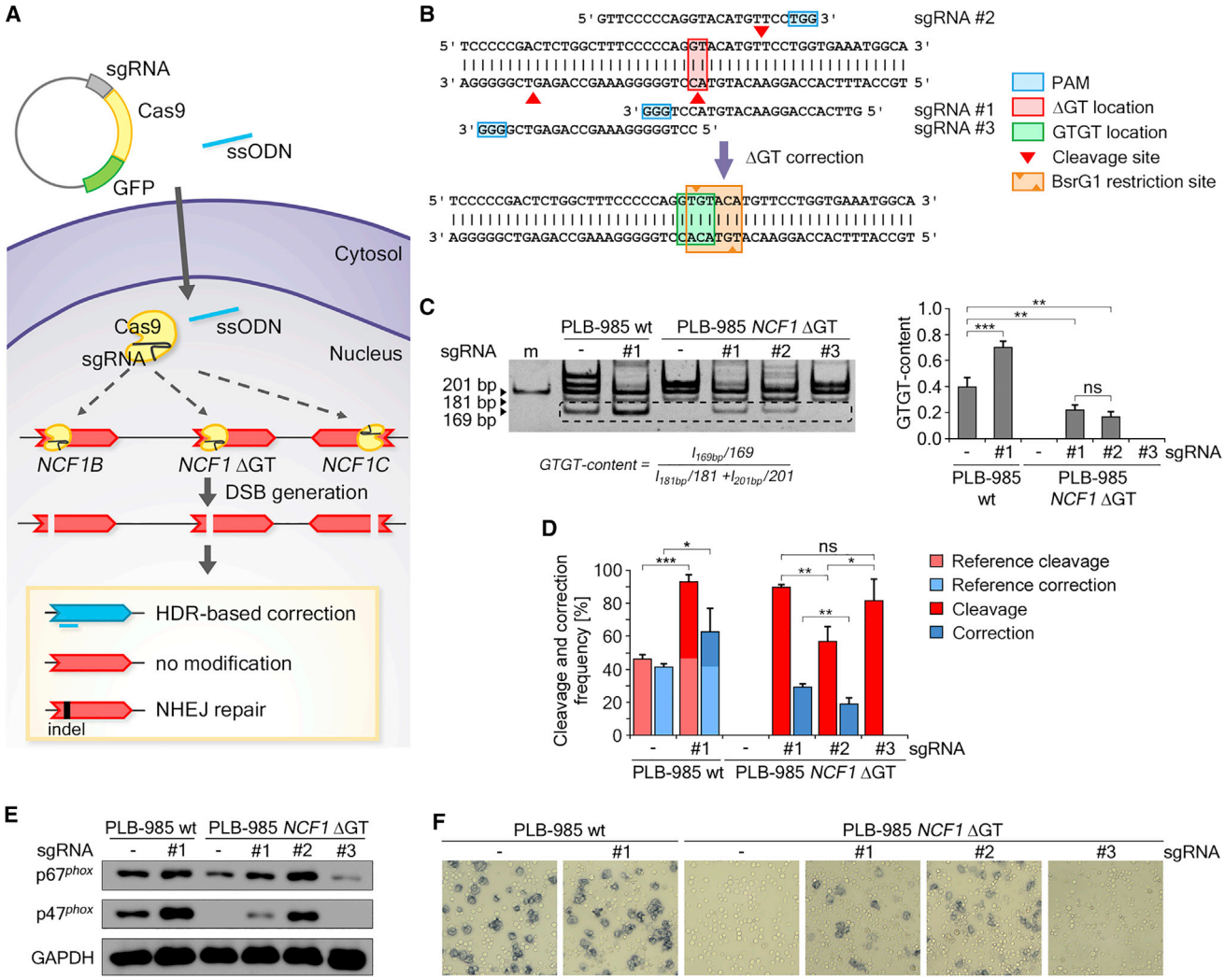

Figure 1. CRISPR-Cas9 Correction of the ΔGT Mutation in PLB-985 WT and PLB-985 *NCF1* ΔGT Cells

(A) Scheme depicting the correction strategy of *NCF1* gene and pseudogene loci by CRISPR-Cas. (B) *NCF1* locus: sequence of tested sgRNAs, cleavage sites for Cas9 (red arrowheads), position of the ΔGT mutation (filled red rectangle), protospacer adjacent motifs (PAMs) (blue rectangles), corrected *NCF1* sequence (green rectangle), digestion sites for BsrG1 (orange arrowheads), and the BsrG1 restriction site (orange rectangle). (C) Polyacrylamide gel of PCR-RFLP analysis of bulk CRISPR-Cas9-treated PLB-985 WT and PLB-985 *NCF1* ΔGT cell lines. Band intensities were analyzed by the displayed formula. The 161-bp band within the dashed rectangle resulted from digestion of corrected *NCF1* (n = 4; bars: means with standard deviations; statistical analysis with unpaired t test with Welch's correction, $^{**}p < 0.01$, $^{***}p < 0.001$). (D) TIDER analysis of cleavage and correction efficiencies for bulk CRISPR-Cas9-treated and untreated PLB-985 WT and PLB-985 *NCF1* ΔGT cell lines (n = 4; bars: means with standard deviations; statistical analysis with unpaired t test with Welch's correction, $^{*}p < 0.05$, $^{**}p < 0.01$, $^{***}p < 0.001$). (E) Western blot of control p67^{phox} (another cytosolic NADPH oxidase subunit, which is complexed with p47^{phox} and p40^{phox}, p47^{phox}, and GAPDH for differentiated bulk CRISPR-Cas9-treated PLB-985 WT and PLB-985 *NCF1* ΔGT cell lines. (F) Light microscopy images of NBT test performed on differentiated bulk CRISPR-Cas9-treated PLB-985 WT and PLB-985 *NCF1* ΔGT cell lines. ns, not significant.

(Figure S3B). Complementarity between the genomic sequences adjacent to the deleted region (Figure 2A) likely contributed to the induction of this deletion upon DSBs repair.

In addition to the observed indel formation, simultaneous CRISPR-Cas9 cleavage of two or three ΔGT-carrying *NCF1* loci that are located on the same chromosome may also lead to large chromosomal rearrangements, which could span the regions between *NCF1B* and *NCF1* (1.5 Mb), *NCF1* and *NCF1C* (0.4 Mb), or *NCF1B* and *NCF1C* (1.9 Mb) (Figure 2B). We therefore quantified copy number variation (CNV) using quantitative PCR (qPCR) of non-repetitive genes, located between *NCF1* loci (*EIF4H* between *NCF1B* and *NCF1*; *WBSCR16* between *NCF1* and *NCF1C*) and genes located outside of the *NCF1* gene and pseudogene loci (*CALN1* upstream of *NCF1B*; *HIP1* downstream of *NCF1C*) (Figures 2B and 2C; Table S5). We identified 8 out of 49 clones (Figure 2C) that exhibited unaltered copy number of *CALN1* and *HIP1* genes located outside the *NCF1* gene and pseudogene loci, but decreased copy number of *EIF4H*

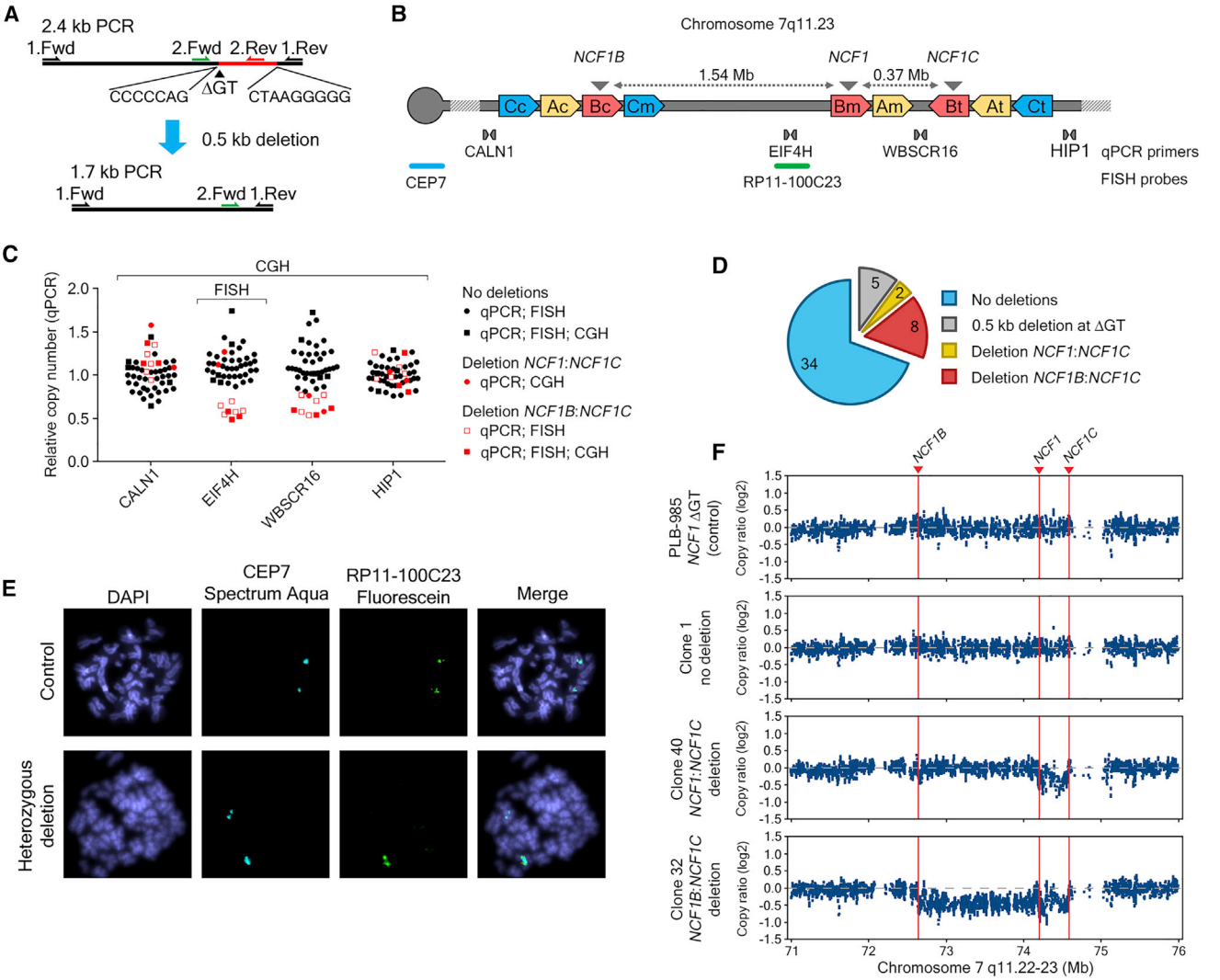

Figure 2. Detection of Chromosomal Aberrations in CRISPR-Cas9-Treated PLB-985 *NCF1* ΔGT Cells

(A) PCR product of *NCF1* gene and pseudogene loci, with indicated primers. ΔGT, deletion-end adjacent partially complementary sequences, and detected deletion (red) between them are indicated. (B) Scheme of chromosome 7 q11.23 fragment: locations of FISH probes, CEP7, binding the centromere of chromosome 7, and RP11-100C23, binding the region between *NCF1B* and *NCF1*, as well as binding sites of four primer pairs used for CNV analysis are shown. A, B and C indicate the amplified chromosomal segments; c (centromeric), m (medial), and t (telomeric) sites. Location of *NCF1*, *NCF1B*, and *NCF1C* in blocks Bm, Bc, and Bt, respectively, is indicated by gray arrowheads. (C) Relative copy number of regions surrounding *NCF1* gene and pseudogene loci in CRISPR-Cas9-treated PLB-985 *NCF1* ΔGT cells determined by qPCR. Clones with deletion between *NCF1B* and *NCF1C* (red squares) and clones with deletion between *NCF1* and *NCF1C* (red circles) are shown. (D) Number of CRISPR-Cas9-treated clones that exhibited no chromosomal aberrations within *NCF1* loci (blue), number of clones with a 0.5-kb deletion at the CRISPR-Cas9 cleavage site (gray), and heterozygous deletions between *NCF1* and *NCF1C* (yellow) and between *NCF1B* and *NCF1C* (red) confirmed by FISH and aCGH. (E) Immunofluorescence microscopy images of FISH analysis for a control clone with centromeric CEP7 Spectrum Aqua binding and with binding sites for RP11-100C23 Fluorescein probe on two chromosomes, as well as a clone with a heterozygous deletion of the region between *NCF1B* and *NCF1* (binding of RP11-100C23 on one chromosome). (F) aCGH of chromosome 7 q11.22-23 region of untreated PLB-985 *NCF1* ΔGT cells and one clone of CRISPR-Cas9-treated PLB-985 *NCF1* ΔGT without (no deletion) and two clones with a heterozygous deletion are shown.

and *WBSCR16*, located between *NCF1* gene and pseudogenes, suggesting the presence of heterozygous deletions between *NCF1B* and *NCF1C*. Interestingly, one clone exhibited decreased CNV only for *WBSCR16*, suggesting a heterozygous deletion between *NCF1* and *NCF1C*. No clones were identified with a homozygous deletion of genes between *NCF1* gene and pseudogene loci, which could result from reduced viability due to homozygous deletion of genes affecting cellular fitness.

Subsequently, all clones were tested for the presence of deletions between *NCF1B* and *NCF1* by fluorescence *in situ* hybridization (FISH) (Figure 2B), and a genome-wide analysis of chromosomal aberrations

was performed on selected clones using microarray-based comparative genomic hybridization (aCGH) (Figures 2C and 2F; Figure S6; Tables S6 and S7). FISH and aCGH analyses confirmed deletions between *NCF1B* and *NCF1C* detected by qPCR, and aCGH identified a second clone with a deletion between *NCF1* and *NCF1C* (Figures 2C–2F). Duplications or chromosomal translocations within these regions were not observed, which suggests that deletions of chromosomal fragments are the predominant chromosomal aberration type after gene editing (see clones 21 and 27 in Figure S6 and Table S7).

DISCUSSION

Although holding great promises to potentially cure monogenetic diseases at their origin, application of gene-editing technologies has also been linked to unpredictable and complex editing outcomes at the targeted site,[27] which is a major hindrance to application of DSB-based gene editing in clinical settings. Our results suggest that CRISPR-Cas9-based gene therapy may indeed efficiently correct mutated *NCF1* and its pseudogenes, and thus rescue the impaired NADPH oxidase activity in ΔGT p47^{phox} CGD patients. However, simultaneous induction of two or three DSBs on a single chromosome can be associated with induction of large chromosomal aberrations that primarily affect the sequences between the targeted loci, as we and others have shown.[28–32]

The genotype of cells with CRISPR-Cas9-induced heterozygous deletions within *NCF1* gene and pseudogene loci resembles the genotype present in patients with Williams syndrome.[33] Haploinsufficiency of genes residing in the deleted region is primarily linked to cardiovascular and neurological manifestations of Williams syndrome. Hemizygosity of the elastin (*ELN*) gene has been linked to the connective-tissue abnormalities and hypertension, whereas hemizygosity of other genes has been associated with impaired visuospatial and motor abilities, as well as with mild-to-moderate intellectual disability. Although Williams syndrome is generally not considered as a cancer-predisposing condition, reports linking the reduced copy number of the *BCL7B* gene that is located between *NCF1B* and *NCF1* to blood malignancies exist.[34,35] A homozygous intra-chromosomal deletion of the region between *NCF1* gene and pseudogene loci has not been observed in clones of CRISPR-Cas9-treated PLB-985 *NCF1* ΔGT cells. Although after gene editing of the *NCF1* loci of a ΔGT p47^{phox} CGD patient, the deleted chromosomal fragments would be restricted to cells of the hematopoietic compartment, their long-term impact and potential adverse functional implications need to be evaluated carefully.

As we demonstrate for pseudogene-associated p47^{phox} CGD, the risk for inducing chromosomal deletions is likely to apply to other diseases caused by mutations associated with highly homologous pseudogenes located on the same chromosome, such as autosomal dominant polycystic kidney disease,[36] type 2 Gaucher disease,[37] or neural tube defects.[38] For later clinical application, future studies will thus require a substantial improvement of gene-editing enzyme delivery protocols, or application of different editing strategies, and development of rigorous post-editing diagnostic protocols. Measures to minimize adverse effects could include tightly controlled transient exposure of the genome to the gene-editing enzyme, application of other gene-editing strategies not generating DSBs, or modulation of repair pathway choice after DSB generation. Base editors[39] inducing *NCF1* exon 2 skipping by targeting the splice acceptor site adjacent to the ΔGT mutation may not lead to reconstitution of the phagocytic NADPH oxidase activity (Figures S1B–S1F); however, introduction of missing nucleotides at the ΔGT mutation without induction of DSBs by prime editors[40] may constitute an appealing treatment alternative.

In conclusion, safety evaluation is of paramount importance for preclinical development of gene-editing-based approaches, especially for pseudogene-related diseases, where targeted genes and homologous pseudogenes are co-localized on the same chromosome. The extent of chromosomal aberrations, as well as their potential effects on the patient's health, should be carefully addressed in preclinical studies on genome-editing gene therapy approaches, especially for pseudogene-related diseases (Table S1). As to the current state of the art, the application of gene-editing technology for treatment of pseudogene-related genetic disorders should therefore be limited to those cases in which the therapy provides immediate amelioration of life-threatening symptoms or the therapeutic benefit for the patient balances out the risk for potential adverse effects.

MATERIALS AND METHODS

Plasmid Construction

The sgRNA sequences were designed using the Optimized CRISPR Design (F. Zhang laboratory, MIT, 2015; http://zlab.bio/guide-design-resources). Single-stranded DNA oligonucleotides were obtained from Microsynth (Balgach, Switzerland), cloned into pSpCas9(BB)-2A-GFP (PX458) (F. Zhang, Addgene plasmid #48138),[41] and the plasmid sequence was confirmed by Sanger sequencing (Microsynth).

Cell Culture Conditions

PLB-985 WT and PLB-985 *NCF1* ΔGT cell lines[21] were cultured in RPMI 1640 medium (PAN-Biotech, Aidenbach, Germany), supplemented with 10% (v/v) fetal calf serum (FCS) (PAN-Biotech), 100 U/mL penicillin, and 100 μg/mL streptomycin (Thermo Fisher Scientific, Reinach, Switzerland). For granulocytic differentiation, cells were cultured for 7 days in RPMI 1640 medium supplemented with 5% (v/v) FCS, 100 U/mL penicillin, 100 μg/mL streptomycin, and 0.5% (v/v) *N,N*-dimethylformamide (DMF) (Sigma Aldrich, Buchs, Switzerland). Throughout all experiments, cells were grown at 37°C in a humidified atmosphere containing 5% (v/v) CO_2.

CRISPR-Cas9 Treatment of the PLB-985 *NCF1* ΔGT Cell Line

PX458 plasmids (15–40 μg) expressing sgRNA, Cas9, and GFP proteins were delivered into 2 × 10^6 PLB-985 WT or PLB-985 *NCF1* ΔGT cells by nucleofection, using the Amaxa Cell Nucleofector Kit V and Amaxa Nucleofector II, program C-023 (Lonza, Basel, Switzerland), along with a 100-nt ssODN (Microsynth) at a final concentration of 3 μM (Figure 1A). The sequence of the ssODN was: 5′-GCC TCT TTG GAG GCT GAA TGG GGT CCC CCG ACT

CTG GCT TTC CCC CAG GTG TAC ATG TTC CTG GTG AAA TGG CAG GAC CTG TCG GAG AAG GTG GTC TAC C-3′. The locations of the binding sites for sgRNA are presented in Figure 1B. Nucleofected cells were supplemented with 500 µL growth medium and incubated at room temperature for 10 min, and cells were transferred to 10 mL growth medium thereafter. 1 µM SCR7 (BioVision, Milpitas, CA, USA) was added 3–4 h after nucleofection, and cells were cultured for 48 h. GFP-positive cells were sorted into a bulk culture (FACSAria III FCF; Becton Dickinson, Allschwil, Switzerland) in preconditioned, sterile filtered growth medium supplemented with 1 µM SCR7. Sorted cells were expanded for 1 month, and individual clones were generated by limiting dilution.

Assessment of Correction Efficacy by PCR-RFLP and TIDER

Genomic DNA of CRISPR-Cas9-treated cells was isolated using DNeasy Blood & Tissue Kit (QIAGEN, Hombrechtikon, Switzerland). Correction efficiency was assessed by PCR-RFLP method, as described previously.[22] In brief, PCR co-amplification products of *NCF1*, *NCF1B*, and *NCF1C* were digested with BsrG1 and Pst1 restriction enzymes, and developed by electrophoresis in a 7.5% polyacrylamide gel. GTGT content was calculated based on size-normalized band intensities. The band intensity 169 bp was divided by the sum of band intensities 181 and 201 bp (Figure 1C).

TIDER analysis[23] was performed using an online tool (https://tider.deskgen.com/) to assess CRISPR-Cas9 editing efficiency. Approximately 590 bp PCR products of *NCF1* and its pseudogenes were amplified using the forward primer, 5′-CCA AGGT CTC AAG CAA TTC TCC-3′, and the reverse primer, 5′-CCA AAG GGT GGA GCT GGA AC-3′. TIDER analysis was performed on the Sanger sequencing chromatograms using the default parameters of the tool.

SMRT Sequencing

Barcoded PCR co-amplification products derived from the CRISPR-Cas9-treated PLB-985 *NCF1* ΔGT clones (i.e., ΔGT carrying *NCF1* and its pseudogenes) had a size of approximately 2.4 kb and were produced using combinations of the following barcoded forward (Fwd) and reverse (Rev) primers: Fwd1, 5′-TTA GGT CTA GGA TCC AGT CAA GGA T-3′; Fwd2, 5′-AAA GGA TCC AGT CAA GGA TCA ATG T-3′; Fwd3, 5′-TTT TCA GGT CTA GGA TCC AGT CAA-3′; Rev1, 5′-TTA GGT TCT GGG AGA TCC TGT CT-3′; Rev2, 5′-AAG TTC TGG GAG ATC CTG TCT GTT-3′; Rev3, 5′-CCA GCA GGT GCA TTT ATT TGG G-3′. Gel-purified amplification products were pooled and analyzed by the Functional Genomics Center Zurich, University of Zurich, and ETH Zurich, Zurich, Switzerland, as described before.[21]

Western Blot

Protein isolation from differentiated PLB-985 WT, PLB-985 *NCF1* ΔGT, and CRISPR-Cas9-treated PLB-985 WT or PLB-985 *NCF1* ΔGT cells was performed as described previously.[42] In brief, cells were homogenized in a modified radioimmunoprecipitation assay (RIPA) lysis buffer and centrifuged for 10 min at 13,000 × *g*. Protein content in the supernatant was analyzed by Bradford assay (Sigma Aldrich). 10 µg total protein was denatured by boiling in a modified Laemmli loading buffer, separated by SDS-PAGE using 10% polyacrylamide gel, and wet-transferred onto Amersham Protran Premium NC nitrocellulose membrane (GE Healthcare Life Sciences, UK). The membrane was blocked with 3% skim milk and immune stained using the following primary antibodies: mouse anti-human $p47^{phox}$ monoclonal antibody clone 1 (Becton Dickinson, Allschwil, Switzerland), mouse anti-human $p67^{phox}$ monoclonal antibody clone D-6, or mouse anti-human GAPDH monoclonal antibody (0411) (both from Santa Cruz Biotechnology, Heidelberg, Germany). The membrane was incubated overnight with primary antibodies diluted 1:500 in an antibody buffer at 4°C, followed by 1-h incubation at room temperature with the mouse IgG kappa binding protein conjugated to horseradish peroxidase (Santa Cruz Biotechnology) diluted 1:3,000. The signal was developed by incubation of the membrane in SuperSignal West Pico PLUS Chemiluminescent Substrate (Thermo Fisher Scientific), visualized with ImageQuant LAS 4000 Biomolecular Imager (GE Healthcare Life Sciences, UK). Densitometric analysis of protein bands was performed using ImageJ.[43]

NBT Test

Differentiated PLB-985 WT, PLB-985 *NCF1* ΔGT, and CRISPR-Cas9-treated clones of PLB-985 *NCF1* ΔGT cells were incubated in 100 µg/mL phorbol 12-myristate 13-acetate (PMA) (Sigma-Aldrich) and 200 ng/mL NBT for 30 min at 37°C and 5% CO_2 followed by cell fixation in 1% (w/v) formaldehyde. Fixed cells were analyzed visually for the presence of formazan precipitates using a Leica DM IL Fluo light microscope equipped with a DFC420 digital camera and LEICA application suite acquisition software (Leica Microsystems, Glattbrugg, Switzerland).

Chemiluminescence Assay

Chemiluminescence assay was performed on differentiated CRISPR-Cas9-treated PLB-985 cells in 96-well plates. A total of 1×10^5 cells/well were mixed with 200 µM luminol and 200 ng/mL PMA. Chemiluminescence signal was recorded with a Mithras LB 940 Multimode Microplate Reader (Berthold Technologies, Zug, Switzerland).

CNV Assessment by qPCR

The CNV of genomic locations surrounding the *NCF1* gene and pseudogene loci in individual clones of CRISPR-Cas9-treated PLB-985 *NCF1* ΔGT cells was assessed by qPCR. Primer sequences are listed in Table S5, and primer annealing locations are displayed in Figure 2B. qPCR was performed with the QuantStudio 7 Flex Real-Time PCR System (Thermo Fisher Scientific) in 384-well plates, using 2.5 ng/µL genomic DNA in a total reaction volume of 10 µL, 500 nM forward and reverse primers, and SsoAdvanced Universal SYBR Green Supermix (Bio-Rad Laboratories, Cressier, Switzerland). PCR conditions included initial denaturation at 95°C for 3 min, 40 cycles of 30-s denaturation at 95°C, 30-s primer annealing at 65°C, and 15-s elongation at 72°C. Obtained mean cycle threshold (Ct) values of three measurements from individual plates were used for calculation of mean Ct values of at least three independent

measurements. Relative copy number values of tested genomic regions were calculated using the $2^{-\Delta\Delta Ct}$ method.[44]

FISH

Chromosome preparations of individual CRISPR-Cas9-treated PLB-985 *NCF1* ΔGT clones were performed according to the manufacturers' instructions. In brief, cells were incubated in hypotonic 0.075 M KCl solution for 30 min at 37°C, followed by dropwise fixation, and subsequent three rounds of washing with fixative solution (methanol:acetic acid; v/v 3:1 ratio). Fixed cells were dropped on a microscopic slide and hybridized with FISH probes. The FISH probes used for hybridization were a chromosome 7 centromere binding probe Vysis CEP7, labeled with Spectrum Aqua (Abbott, Abbott Molecular, Baar, Switzerland), and a BAC library probe RP11-100C23, conjugated to Green 5-Fluorescein dUTP (Empire Genomics, Buffalo, NY, USA). The slides were denatured at 75°C for 5 min, followed by overnight hybridization at 37°C and humid conditions using a Leica ThermoBrite System (Biosystems Switzerland, Muttenz, Switzerland). Then the slides were rinsed with a 0.4× saline sodium citrate (SSC)/0.3% (v/v) IGEPAL buffer (Sigma Aldrich) for 120 s at 72°C ± 2°C and 2× SSC/0.1% (v/v) IGEPAL (Sigma-Aldrich) for 60 s at room temperature. The slides were air-dried, and the nuclei of hybridized cells were visualized with Vectashield Mounting Medium containing DAPI (REACTOLAB, Servion, Switzerland). Microscopic images were acquired using the Axio Imager.Z2 microscope (Carl Zeiss, Feldbach, Switzerland) and analyzed using Isis software (MetaSystems Hard & Software, Altlussheim, Germany). For each tested clone, at least 200 interphase nuclei were analyzed.

aCGH

The PLB-985 *NCF1* ΔGT cell line, as well as selected CRISPR-Cas9-treated PLB-985 *NCF1* ΔGT clones, were subjected to aCGH using the CytoScan HD Array Kit (Affymetrix, Thermo Fisher Scientific, Schlieren, Switzerland) according to the manufacturer's protocol. Results were analyzed with the Chromosome Analysis Suite (ChAS) software (version 3.1.1.27; Affymetrix, Thermo Fisher Scientific).

Statistical Analysis

Statistical analysis was performed using GraphPad Prism 7.03 (GraphPad Software, La Jolla, CA, USA).

SUPPLEMENTAL INFORMATION

Supplemental Information can be found online at https://doi.org/10.1016/j.omtm.2020.04.015.

AUTHOR CONTRIBUTIONS

D.W., U.S., and J.R. designed the experiments, designed figures, and wrote the manuscript; D.W. made the figures and performed the experiments with help of O.P., F.R., R.S.P., and J.T.; M.J. and J.T. gave advice for the experiments and revised the manuscript.

CONFLICTS OF INTEREST

The authors declare no competing interests.

ACKNOWLEDGMENTS

This study was supported by the CGD Society (grant no. CGDS16/01), Hochspezialisierte Medizin Schwerpunkt Immunologie (HSM-2-Immunologie), and the Gottfried und Julia Bangerter-Rhyner-Stiftung. D.W. received a research grant from the University of Zurich (Forschungskredit; FK-17-041). O.P. received a research grant from the University of Zurich (Forschungskredit; FK-17-053). J.R. is funded by the Uniscientia Foundation. J.R. and M.J. are supported by the Clinical Research Priority Program ImmuGene of University of Zurich. M.J. is an International Research Scholar of the Howard Hughes Medical Institute and Vallee Scholar of the Bert N & L Kuggie Vallee Foundation. We thank the Functional Genomics Center Zurich, University of Zurich, and ETH Zurich for performing SMRT sequencing, GUIDE-seq, data analysis, and technical support.

REFERENCES

1. Segal, B.H., Leto, T.L., Gallin, J.I., Malech, H.L., and Holland, S.M. (2000). Genetic, biochemical, and clinical features of chronic granulomatous disease. Medicine (Baltimore) *79*, 170–200.
2. Bianchi, M., Niemiec, M.J., Siler, U., Urban, C.F., and Reichenbach, J. (2011). Restoration of anti-Aspergillus defense by neutrophil extracellular traps in human chronic granulomatous disease after gene therapy is calprotectin-dependent. J. Allergy Clin. Immunol. *127*, 1243–1252.e7.
3. Bianchi, M., Hakkim, A., Brinkmann, V., Siler, U., Seger, R.A., Zychlinsky, A., and Reichenbach, J. (2009). Restoration of NET formation by gene therapy in CGD controls aspergillosis. Blood *114*, 2619–2622.
4. Noack, D., Rae, J., Cross, A.R., Ellis, B.A., Newburger, P.E., Curnutte, J.T., and Heyworth, P.G. (2001). Autosomal recessive chronic granulomatous disease caused by defects in NCF-1, the gene encoding the phagocyte p47-phox: mutations not arising in the NCF-1 pseudogenes. Blood *97*, 305–311.
5. Roos, D., de Boer, M., Kuribayashi, F., Meischl, C., Weening, R.S., Segal, A.W., Ahlin, A., Nemet, K., Hossle, J.P., Bernatowska-Matuszkiewicz, E., and Middleton-Price, H. (1996). Mutations in the X-linked and autosomal recessive forms of chronic granulomatous disease. Blood *87*, 1663–1681.
6. Görlach, A., Lee, P.L., Roesler, J., Hopkins, P.J., Christensen, B., Green, E.D., Chanock, S.J., and Curnutte, J.T. (1997). A p47-phox pseudogene carries the most common mutation causing p47-phox- deficient chronic granulomatous disease. J. Clin. Invest. *100*, 1907–1918.
7. Hockenhull, E.L., Carette, M.J., Metcalfe, K., Donnai, D., Read, A.P., and Tassabehji, M. (1999). A complete physical contig and partial transcript map of the Williams syndrome critical region. Genomics *58*, 138–145.
8. van den Berg, J.M., van Koppen, E., Ahlin, A., Belohradsky, B.H., Bernatowska, E., Corbeel, L., Español, T., Fischer, A., Kurenko-Deptuch, M., Mouy, R., et al. (2009). Chronic granulomatous disease: the European experience. PLoS ONE *4*, e5234.
9. Siler, U., Paruzynski, A., Holtgreve-Grez, H., Kuzmenko, E., Koehl, U., Renner, E.D., Alhan, C., de Loosdrecht, A.A., Schwäble, J., Pfluger, T., et al. (2015). Successful Combination of Sequential Gene Therapy and Rescue Allo-HSCT in Two Children with X-CGD - Importance of Timing. Curr. Gene Ther. *15*, 416–427.
10. Sen, K., and Ghosh, T.C. (2013). Pseudogenes and their composers: delving in the 'debris' of human genome. Brief. Funct. Genomics *12*, 536–547.
11. Bischof, J.M., Chiang, A.P., Scheetz, T.E., Stone, E.M., Casavant, T.L., Sheffield, V.C., and Braun, T.A. (2006). Genome-wide identification of pseudogenes capable of disease-causing gene conversion. Hum. Mutat. *27*, 545–552.
12. Sweeney, C.L., Zou, J., Choi, U., Merling, R.K., Liu, A., Bodansky, A., Burkett, S., Kim, J.W., De Ravin, S.S., and Malech, H.L. (2017). Targeted Repair of CYBB in X-CGD iPSCs Requires Retention of Intronic Sequences for Expression and Functional Correction. Mol. Ther. *25*, 321–330.
13. Klatt, D., Cheng, E., Philipp, F., Selich, A., Dahlke, J., Schmidt, R.E., Schott, J.W., Büning, H., Hoffmann, D., Thrasher, A.J., and Schambach, A. (2019). Targeted

Repair of p47-CGD in iPSCs by CRISPR/Cas9: Functional Correction without Cleavage in the Highly Homologous Pseudogenes. Stem Cell Reports *13*, 590–598.

14. Zou, J., Sweeney, C.L., Chou, B.K., Choi, U., Pan, J., Wang, H., Dowey, S.N., Cheng, L., and Malech, H.L. (2011). Oxidase-deficient neutrophils from X-linked chronic granulomatous disease iPS cells: functional correction by zinc finger nuclease-mediated safe harbor targeting. Blood *117*, 5561–5572.
15. Dreyer, A.-K., Hoffmann, D., Lachmann, N., Ackermann, M., Steinemann, D., Timm, B., Siler, U., Reichenbach, J., Grez, M., Moritz, T., et al. (2015). TALEN-mediated functional correction of X-linked chronic granulomatous disease in patient-derived induced pluripotent stem cells. Biomaterials *69*, 191–200.
16. Merling, R.K., Sweeney, C.L., Chu, J., Bodansky, A., Choi, U., Priel, D.L., Kuhns, D.B., Wang, H., Vasilevsky, S., De Ravin, S.S., et al. (2015). An AAVS1-targeted minigene platform for correction of iPSCs from all five types of chronic granulomatous disease. Mol. Ther. *23*, 147–157.
17. De Ravin, S.S., Reik, A., Liu, P.Q., Li, L., Wu, X., Su, L., Raley, C., Theobald, N., Choi, U., Song, A.H., et al. (2016). Targeted gene addition in human CD34(+) hematopoietic cells for correction of X-linked chronic granulomatous disease. Nat. Biotechnol. *34*, 424–429.
18. De Ravin, S.S., Li, L., Wu, X., Choi, U., Allen, C., Koontz, S., Lee, J., Theobald-Whiting, N., Chu, J., Garofalo, M., et al. (2017). CRISPR-Cas9 gene repair of hematopoietic stem cells from patients with X-linked chronic granulomatous disease. Sci. Transl. Med. *9*, eaah3480.
19. Merling, R.K., Kuhns, D.B., Sweeney, C.L., Wu, X., Burkett, S., Chu, J., Lee, J., Koontz, S., Di Pasquale, G., Afione, S.A., et al. (2016). Gene-edited pseudogene resurrection corrects p47^{phox}-deficient chronic granulomatous disease. Blood Adv. *1*, 270–278.
20. Sürün, D., Schwäble, J., Tomasovic, A., Ehling, R., Stein, S., Kurrle, N., von Melchner, H., and Schnütgen, F. (2018). High Efficiency Gene Correction in Hematopoietic Cells by Donor-Template-Free CRISPR/Cas9 Genome Editing. Mol. Ther. Nucleic Acids *10*, 1–8.
21. Wrona, D., Siler, U., and Reichenbach, J. (2017). CRISPR/Cas9-generated p47^{phox}-deficient cell line for Chronic Granulomatous Disease gene therapy vector development. Sci. Rep. *7*, 44187.
22. Wrona, D., Siler, U., and Reichenbach, J. (2019). Novel Diagnostic Tool for p47 ^{phox} -Deficient Chronic Granulomatous Disease Patient and Carrier Detection. Mol. Ther. Methods Clin. Dev. *13*, 274–278.
23. Brinkman, E.K., Kousholt, A.N., Harmsen, T., Leemans, C., Chen, T., Jonkers, J., and van Steensel, B. (2018). Easy quantification of template-directed CRISPR/Cas9 editing. Nucleic Acids Res. *46*, e58.
24. Tsai, S.Q., Zheng, Z., Nguyen, N.T., Liebers, M., Topkar, V.V., Thapar, V., Wyvekens, N., Khayter, C., Iafrate, A.J., Le, L.P., et al. (2015). GUIDE-seq enables genome-wide profiling of off-target cleavage by CRISPR-Cas nucleases. Nat. Biotechnol. *33*, 187–197.
25. Maßberg, D., and Hatt, H. (2018). Human Olfactory Receptors: Novel Cellular Functions Outside of the Nose. Physiol. Rev. *98*, 1739–1763.
26. Levene, M.J., Korlach, J., Turner, S.W., Foquet, M., Craighead, H.G., and Webb, W.W. (2003). Zero-mode waveguides for single-molecule analysis at high concentrations. Science *299*, 682–686.
27. Kosicki, M., Tomberg, K., and Bradley, A. (2018). Repair of double-strand breaks induced by CRISPR-Cas9 leads to large deletions and complex rearrangements. Nat. Biotechnol. *36*, 765–771.
28. Traxler, E.A., Yao, Y., Wang, Y.D., Woodard, K.J., Kurita, R., Nakamura, Y., Hughes, J.R., Hardison, R.C., Blobel, G.A., Li, C., and Weiss, M.J. (2016). A genome-editing strategy to treat β-hemoglobinopathies that recapitulates a mutation associated with a benign genetic condition. Nat. Med. *22*, 987–990.
29. Blasco, R.B., Karaca, E., Ambrogio, C., Cheong, T.C., Karayol, E., Minero, V.G., Voena, C., and Chiarle, R. (2014). Simple and rapid in vivo generation of chromosomal rearrangements using CRISPR/Cas9 technology. Cell Rep. *9*, 1219–1227.
30. Maddalo, D., Manchado, E., Concepcion, C.P., Bonetti, C., Vidigal, J.A., Han, Y.C., Ogrodowski, P., Crippa, A., Rekhtman, N., de Stanchina, E., et al. (2014). In vivo engineering of oncogenic chromosomal rearrangements with the CRISPR/Cas9 system. Nature *516*, 423–427.
31. Long, J., Hoban, M.D., Cooper, A.R., Kaufman, M.L., Kuo, C.Y., Campo-Fernandez, B., Lumaquin, D., Hollis, R.P., Wang, X., Kohn, D.B., and Romero, Z. (2018). Characterization of Gene Alterations following Editing of the β-Globin Gene Locus in Hematopoietic Stem/Progenitor Cells. Mol. Ther. *26*, 468–479.
32. Brunet, E., and Jasin, M. (2018). Induction of Chromosomal Translocations with CRISPR-Cas9 and Other Nucleases: Understanding the Repair Mechanisms That Give Rise to Translocations. Adv. Exp. Med. Biol. *1044*, 15–25.
33. Pober, B.R. (2010). Williams-Beuren syndrome. N. Engl. J. Med. *362*, 239–252.
34. Decimi, V., Fazio, G., Dell'Acqua, F., Maitz, S., Galbiati, M., Rizzari, C., Biondi, A., Cazzaniga, G., and Selicorni, A. (2016). Williams syndrome and mature B-Leukemia: A random association? Eur. J. Med. Genet. *59*, 634–640.
35. Kimura, R., Ishii, Y., Tomiwa, K., Awaya, T., Nakata, M., Kato, T., Okazaki, S., Heike, T., and Hagiwara, M. (2018). Williams-Beuren Syndrome as a Potential Risk Factor for Burkitt Lymphoma. Front. Genet. *9*, 368.
36. Bogdanova, N., Markoff, A., Gerke, V., McCluskey, M., Horst, J., and Dworniczak, B. (2001). Homologues to the first gene for autosomal dominant polycystic kidney disease are pseudogenes. Genomics *74*, 333–341.
37. Horowitz, M., Wilder, S., Horowitz, Z., Reiner, O., Gelbart, T., and Beutler, E. (1989). The human glucocerebrosidase gene and pseudogene: structure and evolution. Genomics *4*, 87–96.
38. Campbell, I.G., Jones, T.A., Foulkes, W.D., and Trowsdale, J. (1991). Folate-binding protein is a marker for ovarian cancer. Cancer Res. *51*, 5329–5338.
39. Rees, H.A., and Liu, D.R. (2018). Base editing: precision chemistry on the genome and transcriptome of living cells. Nat. Rev. Genet. *19*, 770–788.
40. Anzalone, A.V., Randolph, P.B., Davis, J.R., Sousa, A.A., Koblan, L.W., Levy, J.M., Chen, P.J., Wilson, C., Newby, G.A., Raguram, A., and Liu, D.R. (2019). Search-and-replace genome editing without double-strand breaks or donor DNA. Nature *576*, 149–157.
41. Ran, F.A., Hsu, P.D., Wright, J., Agarwala, V., Scott, D.A., and Zhang, F. (2013). Genome engineering using the CRISPR-Cas9 system. Nat. Protoc. *8*, 2281–2308.
42. Huwiler, A., and Pfeilschifter, J. (1994). Stimulation by extracellular ATP and UTP of the mitogen-activated protein kinase cascade and proliferation of rat renal mesangial cells. Br. J. Pharmacol. *113*, 1455–1463.
43. Schneider, C.A., Rasband, W.S., and Eliceiri, K.W. (2012). NIH Image to ImageJ: 25 years of image analysis. Nat. Methods *9*, 671–675.
44. Livak, K.J., and Schmittgen, T.D. (2001). Analysis of relative gene expression data using real-time quantitative PCR and the 2(-Δ Δ C(T)) Method. Methods *25*, 402–408.

OMTM, Volume *17*

Supplemental Information

CRISPR-Directed Therapeutic Correction at the *NCF1* Locus Is Challenged by Frequent Incidence of Chromosomal Deletions

Dominik Wrona, Oleksandr Pastukhov, Robert S. Pritchard, Federica Raimondi, Joëlle Tchinda, Martin Jinek, Ulrich Siler, and Janine Reichenbach

Supplemental Figures

Non-homologous end joining (NHEJ)-based repair of CRIPSR-Cas9-induced double-strand breaks (DSBs) at the ΔGT mutation within mutated *NCF1* locus and its pseudogenes generates a variety of indel mutations. Some of these mutations lead to recovery of the *NCF1* gene open reading frame, and may result in expression of a truncated but functional version of p47^{phox} (see **Table S4, and Figure S1**).

Figure S1

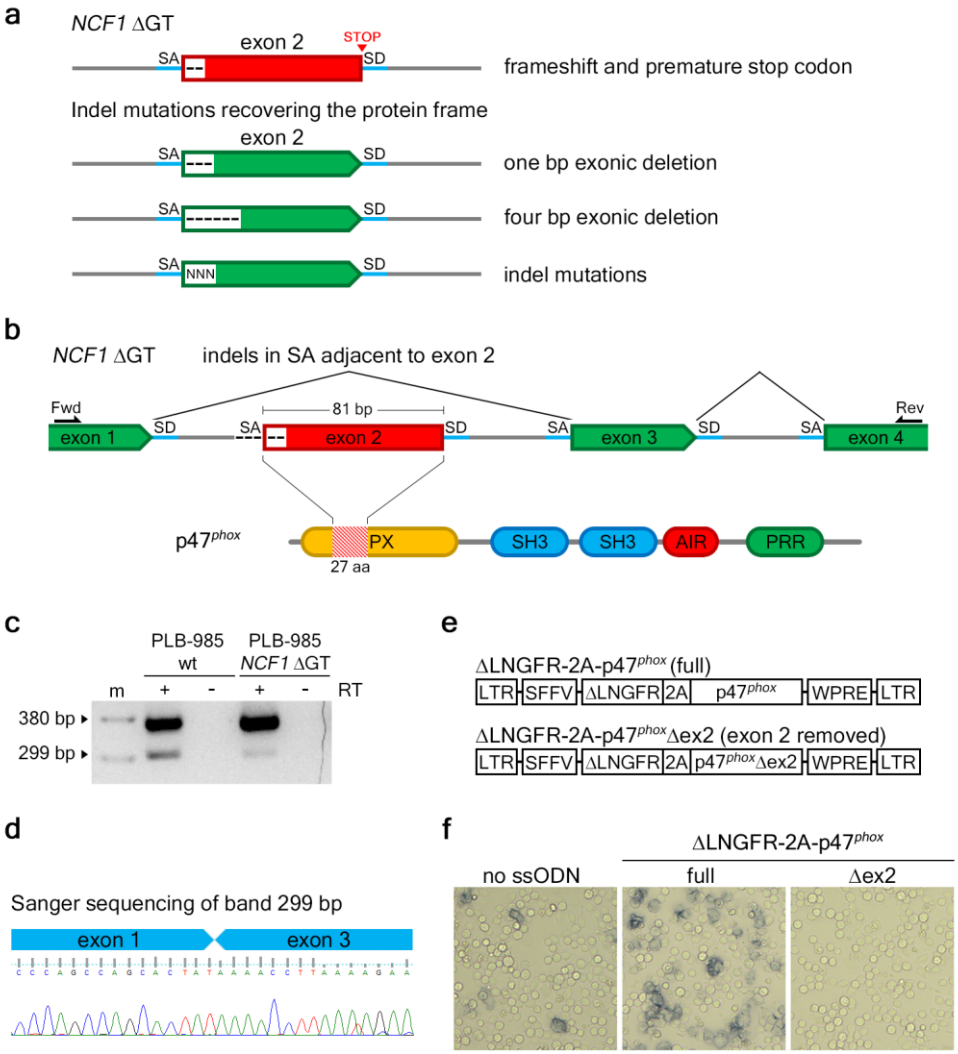

Reconstitution of NADPH oxidase activity upon CRISPR-Cas9-treatment of PLB-985 *NCF1* ΔGT cell line in the absence of corrective template

(**a**) Scheme of exon 2 (red) of the *NCF1* locus, carrying the ΔGT mutation (--), with indicated location of stop codon, as well as of *NCF1* exon 2 with possible open reading frame-recovering indel mutations: --- (deletion of 1bp truncates p47^{phox} by 1 amino acid) or ------ (deletion of 4 bp truncates p47^{phox} by 2 amino acids), NNN (insertion of 2 bp, or complex indel mutation).

(**b**) Scheme of *NCF1* gene fragment including exons 1-4 (top), as well as scheme of p47^{phox} protein with distinct protein domains. *NCF1* exon 2 consists of 81 bp that encode for 27 amino acids of the p47^{phox} membrane phospholipid binding phox homology (PX) domain. Since the ΔGT mutation is localized at the beginning of exon 2, CRISPR-Cas9-induced indel mutations can potentially lead to disruption of the adjacent splicing acceptor site (SA), and as a consequence to alternative splicing of *NCF1* transcript lacking exon 2 (exon skipping). This in turn may lead to expression of a truncated, yet in-frame version of p47^{phox}. Other depicted domains of p47^{phox} are Src homology 3 domain (SH3), auto-inhibitory region (AIR), and proline-rich region (PRR).

(**c**) Alternative splicing of *NCF1* mRNA in granulocytes differentiated from the PLB-985 *NCF1* ΔGT cell line leads to the presence of *NCF1* transcript without exon 2. PLB-985 wt and PLB-985 *NCF1* ΔGT were differentiated into

granulocytes, and total RNA was isolated from the cells (RNeasy Mini Kit, Qiagen). The presence of correctly spliced *NCF1* transcripts (380bp RT-PCR product), and of exon 2 deficient transcripts (299bp RT-PCR product) in PLB-985 wt and PLB-985 *NCF1* ΔGT was confirmed by reverse transcription. PCR reaction was performed using primers indicated in b: forward (Fwd: ACA CCT TCA TCC GTC ACA TCG) and reverse (Rev: CGT GGG GAG CTT GAG GTC AT, following cDNA generation with RevertAid RT Reverse Transcription Kit (Thermo Fisher Scientific).
(**d**) Sanger sequencing of RT-PCR products confirmed the presence of exon 2 deficient transcripts. (**e**) γ-retroviral vectors used to express full, or exon 2 deficient p47^{phox} in PLB-985 *NCF1* ΔGT cells. The expression cassette between long terminal repeats (LTR) was composed of spleen focus-forming virus (SFFV) promoter, a truncated low-affinity nerve growth factor receptor (ΔLNGFR) surface protein marker, allowing for isolation of successfully transduced cells, and full, or exon 2 deficient *NCF1* cDNA, fused to ΔLNGFR by a 2A self-cleaving peptide.[45] WPRE, woodchuck hepatitis virus posttranscriptional regulatory element.
(**f**, middle and right images) PLB-985 *NCF1* ΔGT cells were transduced with γ-retroviral vectors (schemes in **e**), followed by ΔLNGFR-expressing cells enrichment by fluorescence activated cell sorting (FACS) 24 hours post-transduction, and cultured. The NADPH oxidase activity in differentiated cells was analyzed by NBT test.
(**f**, left image) NBT assay of nucleofected PLB-985 *NCF1* ΔGT cells. Cells were nucleofected as described in Methods of the main text, but without the corrective ssODN template (no ssODN). NBT test was performed on the differentiated bulk culture, and demonstrated reconstitution of ROS production in individual cells.

The results shown in **f** indicate that use of a corrective template for restoration of the NADPH oxidase function is not indispensable (**f**, left image), as suggested by the results observed in another study on X-CGD.[20] On the other hand, *NCF1* exon 2 deficient transcript does not recover the function of the NADPH oxidase (**f**, right image). Only the cells transduced with a vector expressing complete p47^{phox} (**f**, full) reconstituted the activity of the enzyme, whereas the truncated form of p47^{phox} that had exon 2 removed (**f**, Δex2) did not rescue the CGD phenotype. These results indicate that the PX domain, encoded partially by *NCF1* exon 2 is elementary for p47^{phox} protein function, and that expression of p47^{phox} lacking exon 2 due to disruption of the splicing site adjacent to the ΔGT mutation by gene-editing-induced indel mutations does not contribute to the reconstitution of NADPH oxidase function. Therefore, reconstitution of NADPH oxidase function upon CRISPR-Cas9 treatment without corrective template must be the result of created indel mutations, which lead to the expression of an in-frame modified version of p47^{phox}.

Figure S2

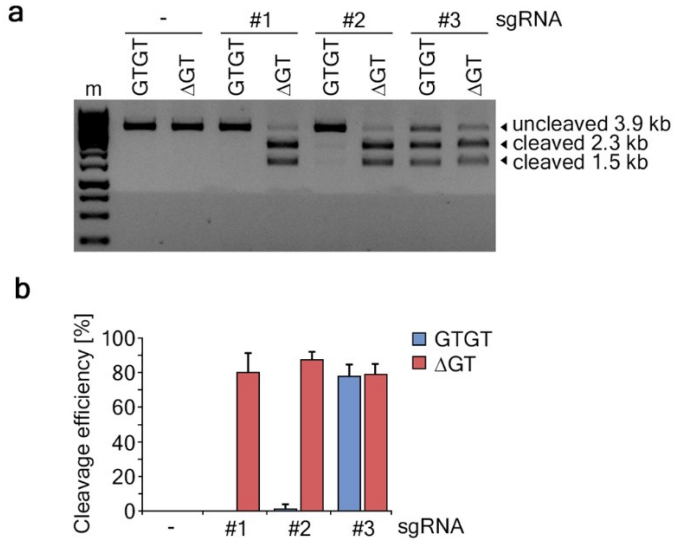

Plasmid DNA cleavage assay to test specificity of sgRNAs

In order to test the specificity of sgRNAs toward the sequence of *NCF1* carrying the GTGT-tetranucleotide or ΔGT mutation, two plasmids with the fragment of the *NCF1* gene or pseudogene sequence spanning the GTGT-tetranucleotide or ΔGT mutation, respectively, were subjected to the plasmid DNA cleavage assay.[46]

Briefly, the plasmids were linearized by restriction digestion with SmaI restriction enzyme (New England Biolabs, Frankfurt am Main, Germany) and subsequently incubated with a 1.5 µM ribonucleoprotein complex of purified SpCas9 and *in vitro* T7 polymerase-transcribed sgRNA. The plasmid cleavage reaction was performed at 37°C for 5 hours in the cleavage buffer (20 mM HEPES pH 7.5, 100 mM KCl, 2 mM $MgCl_2$, 5% (v/v) glycerol, 1 mM DTT, 0.5 mM EDTA). The reaction was stopped with 40 mM EDTA, pH 8.0 followed by sgRNA and Cas9 protein removal with RNase A (Thermo Fisher Scientific, Reinach, Switzerland) and Proteinase K (Roche Diagnostics AG, Rotkreuz, Switzerland) treatment, respectively. RNase A was added to the blocked reaction to reach the final concentration of 0.8 mg/mL and incubated for 1 hour at room temperature. Subsequently, Proteinase K was added to the sample at the final concentration of 1.4 mg/mL and incubated for 30 minutes at room temperature. The samples were developed by agarose electrophoresis.

(**a**) Results of the plasmid DNA cleavage assay developed by agarose electrophoresis. GTGT and ΔGT indicate linearized plasmids (uncleaved 3.9 kb) carrying the GTGT-tetranucleotide or ΔGT mutation, respectively. The bands 'cleaved 2.3 kb' as well as 'cleaved 1.5 kb' result from sgRNA-mediated Cas9 digestion.

(**b**) Quantification of the cleavage efficiency based on band intensities using ImageJ.[43] Bars represent mean cleavage efficiency plus standard deviation of three independent sgRNA transcriptions, ribonucleoprotein complex formations and digestion reactions.

Figure S3

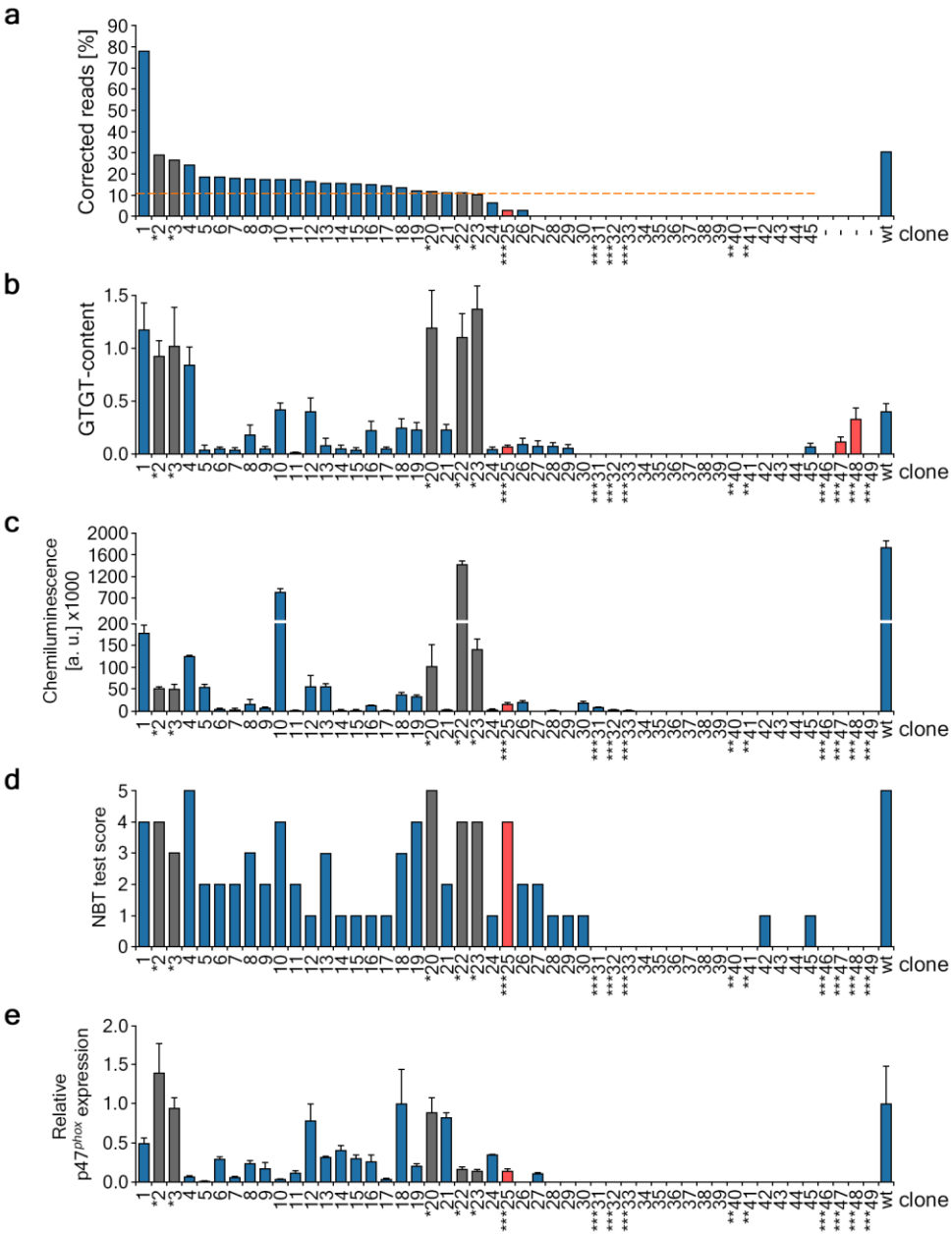

Genetic and functional characterization of individual clones of CRISPR-Cas9-treated PLB-985 *NCF1* ΔGT cell line

Color legend: bars of clones that exhibited no chromosomal aberrations (blue, no asterisk); clones with identified 0.5 kb microdeletion at the CRISPR-Cas9 on-target site (see **Figure 2A**; grey, one asterisk); clones with identified chromosomal deletions between *NCF1* loci (red, two asterisks: deletion identified between *NCF1* and *NCF1C;* three asterisks: deletion identified between *NCF1B* and *NCF1C*).

(**a**) Percentage of SMRT sequencing reads with corrected ΔGT mutation. Mean percentage of corrected reads in Cas9-expressing clones (horizontal orange dashed line).

(**b**) PCR-RFLP analysis of PCR co-amplification products with reconstituted BsrG1 restriction site. The GTGT-content determines how many *NCF1* loci were corrected in the pool of *NCF1* loci present in the genome of CRISPR-Cas9-treated clones. Nota bene, the presence of 0.5 kb microdeletion caused artificially high GTGT-values, as the deletion removes the reverse primer binding site utilized in PCR-PFLP analysis.

(**c**) Chemiluminescence assay performed on clones after differentiation to granulocytes. Bars: area under the curve within the first 30 minutes after activation with PMA, representing the activity of the NADPH oxidase.

(**d**) NBT test performed on clones after differentiation to granulocytes. The NADPH oxidase-dependent deposition of formazan within CRIPSR-Cas9-treated cells was assessed microscopically (NBT test score 0-5; 0: no activity, 5: highest activity; see **Figure S4**).
(**e**) Relative expression of $p47^{phox}$ protein by western blot in corrected clones differentiated to granulocytes, as compared to PLB-985 wt cells. Expression of the phagocytic NADPH oxidase protein components ($gp91^{phox}$, $p22^{phox}$, $p67^{phox}$, $p47^{phox}$, $p40^{phox}$) in PLB-985 cell line is induced by granulocytic differentiation.[47] Band intensities of $p47^{phox}$ were controlled for differentiation status by normalization of the signal by signal of $p67^{phox}$ (see representative western blot membrane in **Figure S5**).
Data represented as means of three measurements plus standard deviation in a-e.

Collectively, this set of experiments demonstrates that around 60% of CRISPR-Cas9-treated PLB-985 *NCF1* ΔGT cells displayed correction of ΔGT mutation in mutated *NCF1* and its pseudogenes, together with restoration of $p47^{phox}$ protein expression and NADPH oxidase function.
Observed levels of ROS generation among the clones were diverse, and not correlated to the number of corrected *NCF1* loci or the level of $p47^{phox}$ protein expression. The reason for this is likely the individual genetic configuration of CRISPR-Cas9-edited *NCF1* loci, as indel mutations can partially rescue NADPH oxidase activity (**Figure S1)**. In addition, correction of mutated *NCF1* and/or pseudogene alleles may be diversely regulated on the level of gene transcription and protein translation. Also, CRISPR-Cas9-induced chromosomal rearrangements may contribute to the observed complex genotype/phenotype of tested clones. Notably, a majority of clones that presented large chromosomal deletions (** and ***) did not display genetic correction, $p47^{phox}$ protein expression, or NADPH oxidase activity.

Figure S4

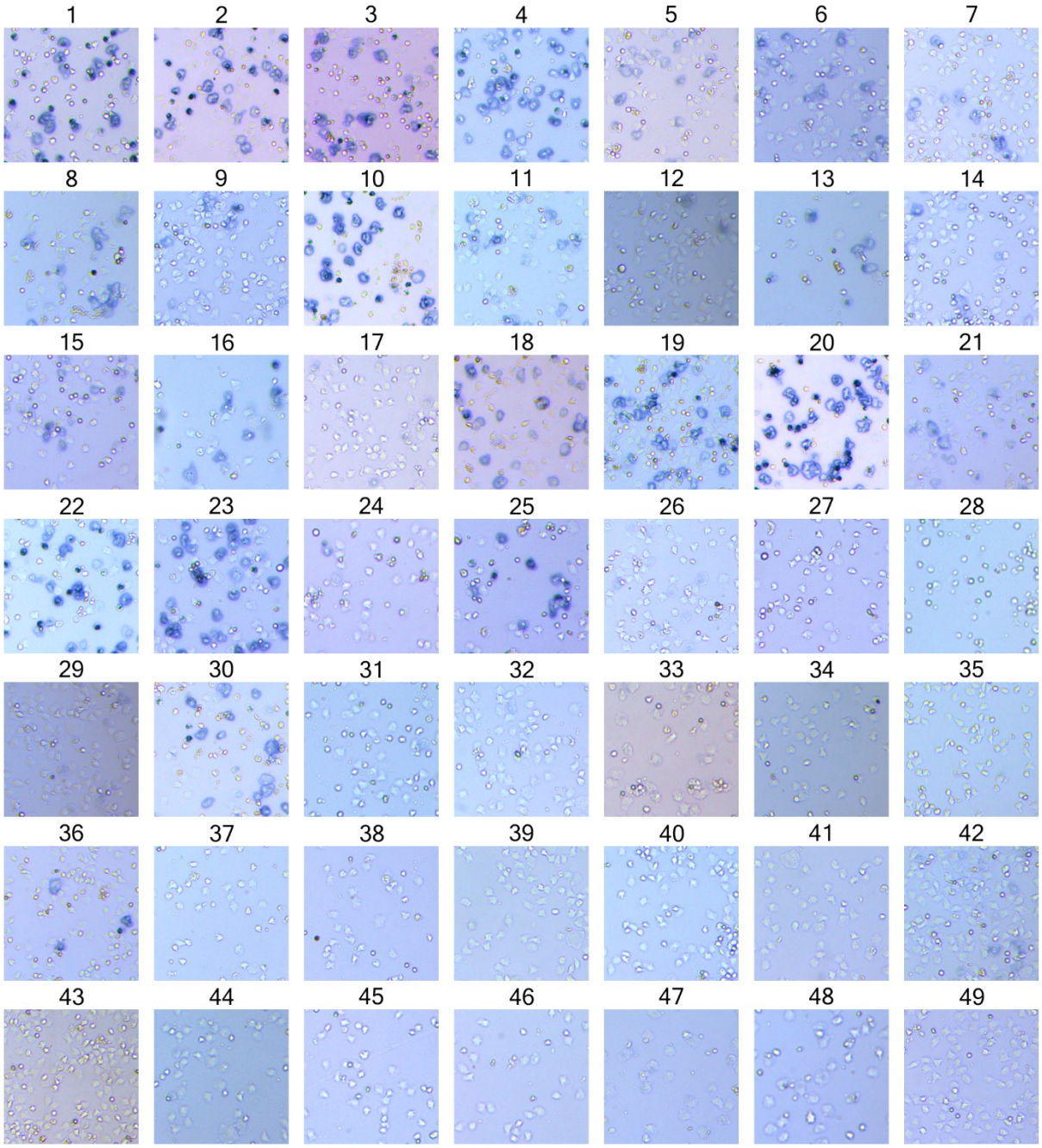

NBT test on individual clones of CRISPR-Cas9-treated PLB-985 *NCF1* ΔGT cell line
Light microscopic images used for the assessment of NADPH oxidase activity in individual clones of CRISPR-Cas9-treated PLB-985 *NCF1* ΔGT cell line after differentiation to granulocytes (NBT score shown in **Figure S3d**). Dark blue precipitates of formazan inside and outside of cells indicate NADPH oxidase-dependent ROS production.

Figure S5

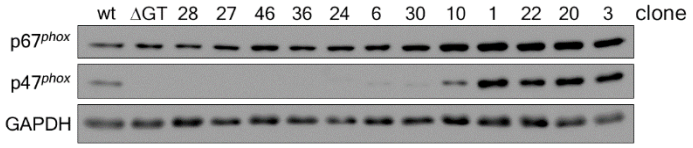

p47*phox* protein expression in selected individual clones of CRISPR-Cas9-treated PLB-985 *NCF1* ΔGT cell line
Western blot of p67*phox*, p47*phox*, and GAPDH in selected clones of CRISPR-Cas9-treated PLB-985 *NCF1* ΔGT cell line after differentiation to granulocytes (**Figure S3e**).

Figure S6

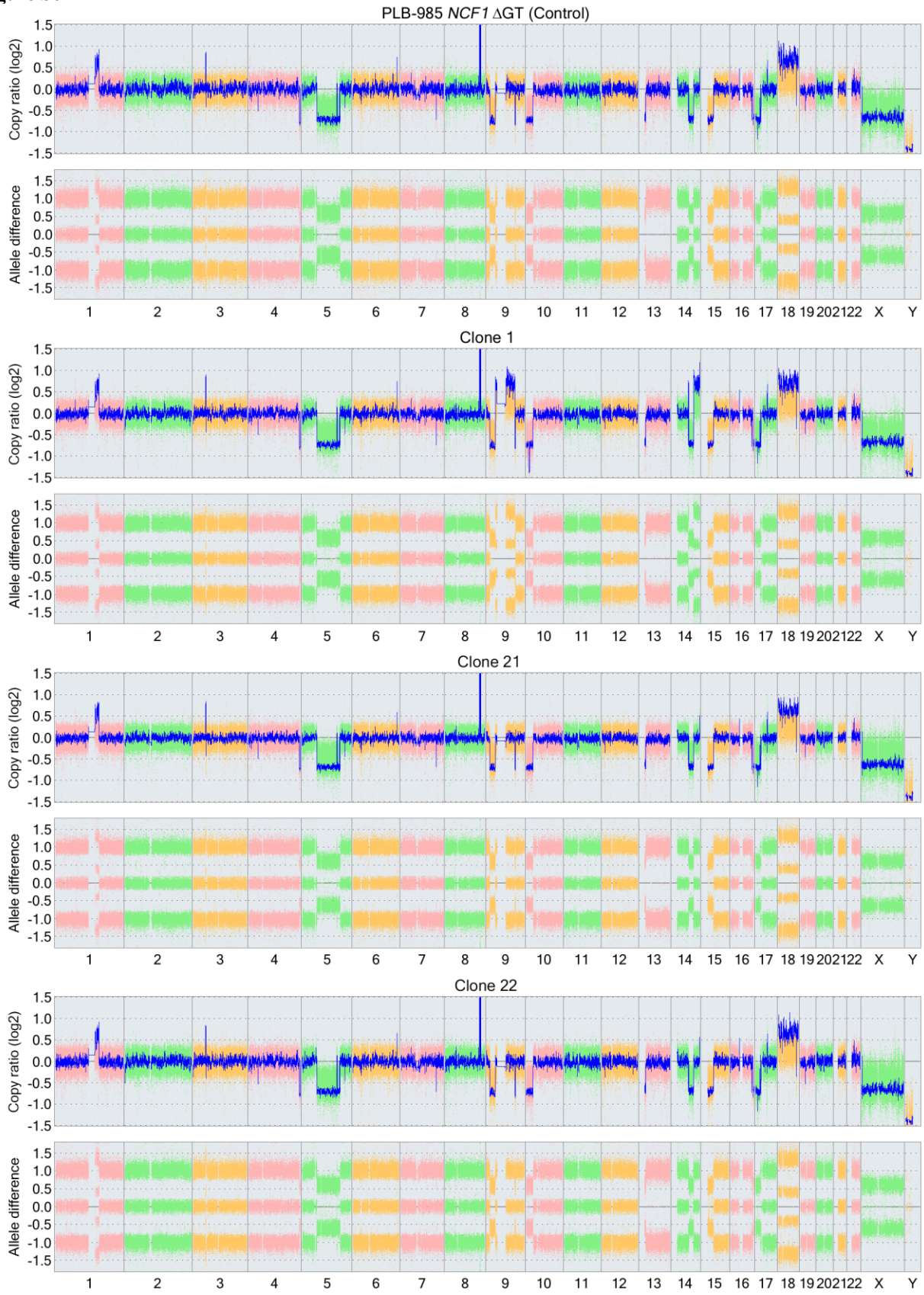
PLB-985 NCF1 ΔGT (Control)
Clone 1
Clone 21
Clone 22
Copy ratio (log2)
Allele difference
1.5
1.0
0.5
0.0
-0.5
-1.0
-1.5
1 2 3 4 5 6 7 8 9 10 11 12 13 14 15 16 17 18 19 20 21 22 X Y

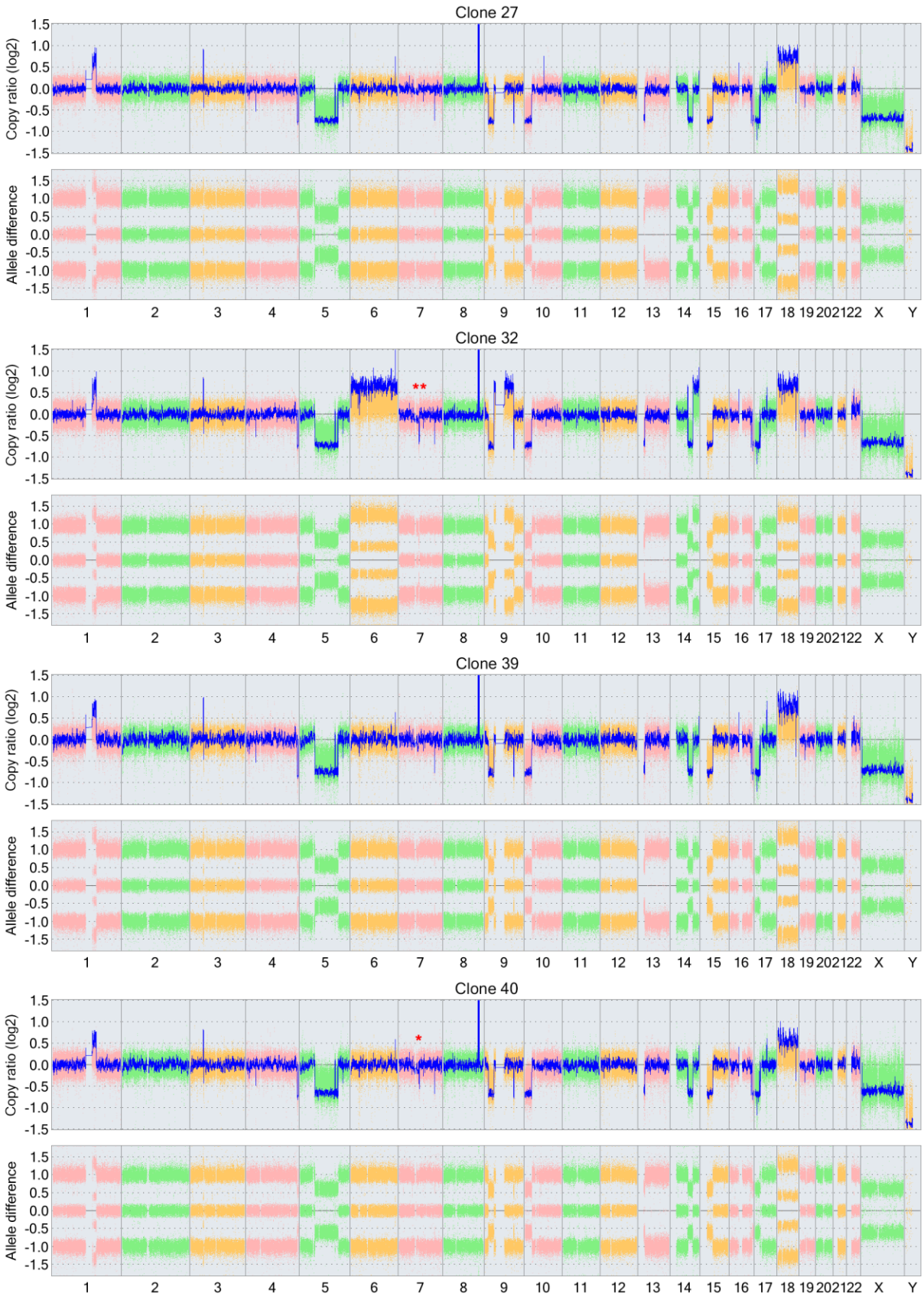
Clone 27
Copy ratio (log2)
Allele difference
Clone 32
**
Clone 39
Clone 40
*
1.5
1.0
0.5
0.0
-0.5
-1.0
-1.5
1 2 3 4 5 6 7 8 9 10 11 12 13 14 15 16 17 18 19 20 21 22 X Y

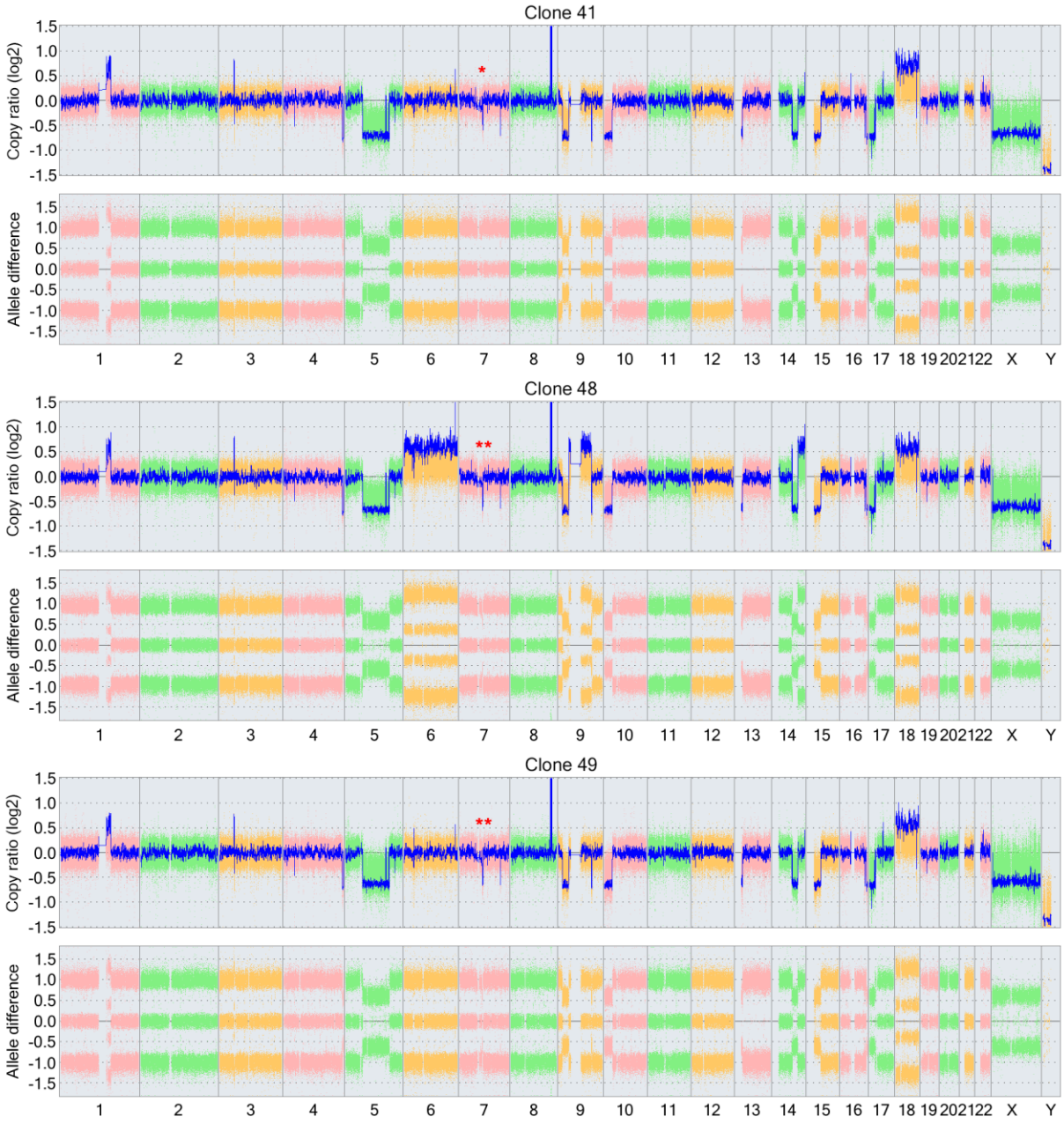

Microarray-based comparative genomic hybridization (aCGH) of selected clones of CRISPR-Cas9-treated PLB-985 *NCF1* ΔGT cell line

Results are compared to the reference genome using the CytoScan™ HD Array. Copy number ratio (log2) as well as allele differences are shown. Chromosome numbers are listed under the graphs. Aberrations localized between the *NCF1* gene and pseudogene loci (chromosome 7) are marked with either one red asterisk (deletion between *NCF1* and *NCF1C*), or two red asterisks (deletion between *NCF1B* and *NCF1C*).

Identified chromosomal aberrations in the genome of PLB-985 *NCF1* ΔGT cell line are listed in **Table S6**. PLB-985 cell line is a sub clone of the HL-60 cell line,[48] and the aCGH array readout for PLB-985 *NCF1* ΔGT cell line retained aberrations characteristic for the parental cell line, including trisomy of chromosome 18 and monosomy of the X chromosome.

De novo alternations found in selected CRISPR-Cas9-treated clones are listed in **Table S7**. Inspection of the break points of duplicated or deleted chromosomal fragments, 20 000 bp window around the break point, confirmed the presence of the targeted sequence within *NCF1* loci located on chromosome 7. Deletions found between these loci most likely result from CRISPR-Cas9-mediated simultaneous induction of DSBs at the on-target sites. On the other

hand, other chromosomal aberrations could not be attributed to off-target CRISPR-Cas9 activity, as there were no sequences identified within the break points with fewer mismatches than 6 nucleotides.

Figure S7

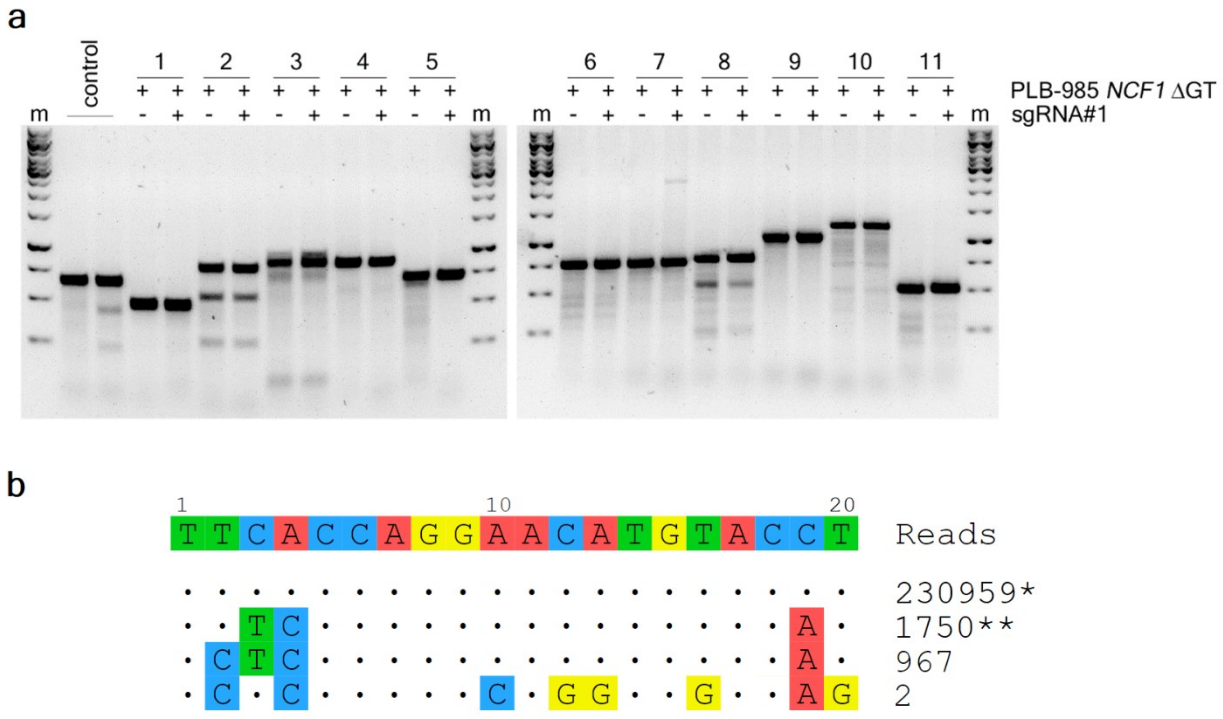

T7 Endonuclease I assay and GUIDE-seq off-target detection

(**a**) The potential off-target sites were predicted with COSMID (CRISPR Off-target Sites with Mismatches, Insertions, and Deletions) analysis tool (https://crispr.bme.gatech.edu/; see **Table S2**).[49] The regions surrounding these sites were PCR amplified from genomic DNA of PLB-985 *NCF1* ΔGT and the bulk culture of CRISPR-Cas9-treated PLB-985 *NCF1* ΔGT cells (sgRNA #1). Corresponding PCR products were mixed in a 1:1 ratio, while PCR amplification products from PLB-985 *NCF1* ΔGT were used as controls along tested samples (total of 200 ng DNA). The lanes marked as 'control' contain PCR products of Control C (lane 2) as well as 1:1 mixture of PCR products of Control C and Control G (lane 3) of the Surveyor® Mutation Detection Kit For Standard Gel Electrophoresis (Integrated DNA Technologies, Leuven, Belgium). The samples were denatured at 95 °C for 5 minutes, slowly renatured, and digested using T7 Endonuclease I (New England Biolabs) according to the manufacturer's instructions.

None of the tested potential off-target sites exhibited additional cleavage, indicating that sgRNA #1 specifically guides Cas9 towards the mutated *NCF1* as well as *NCF1* pseudogenes in PLB-985 *NCF1* ΔGT.

(**b**) PLB-985 *NCF1* ΔGT cells have been nucleofected with a Cas9, GFP and sgRNA #1 encoding plasmid, as described the Methods, in the presence of 10 pmol of Genome-wide Unbiased Identification of DSBs Enabled by Sequencing (GUIDE-seq) dsDNA oligonucleotide. GFP expressing cells were sorted, expanded and subjected to GUIDE-seq analysis.[24] Sequencing was performed using an Illumina MiSeq sequencer (Illumina Inc., San Diego. CA, USA). MiSeq paired-reads were analyzed using guideseq (v1.1b5, mapq = 0) against the human reference genome (Ensembl GRCh38.p10) for identification of off-targets.

The on-target site represents combined reads mapped to all *NCF1* loci (*). Three off-target sequences have been identified by GUIDE-seq, however, the most frequently cleaved off-target (**; 0.76% of the cleavage at the on-target) is represented within five distinct genomic locations (**Table S3**).

Figure S8

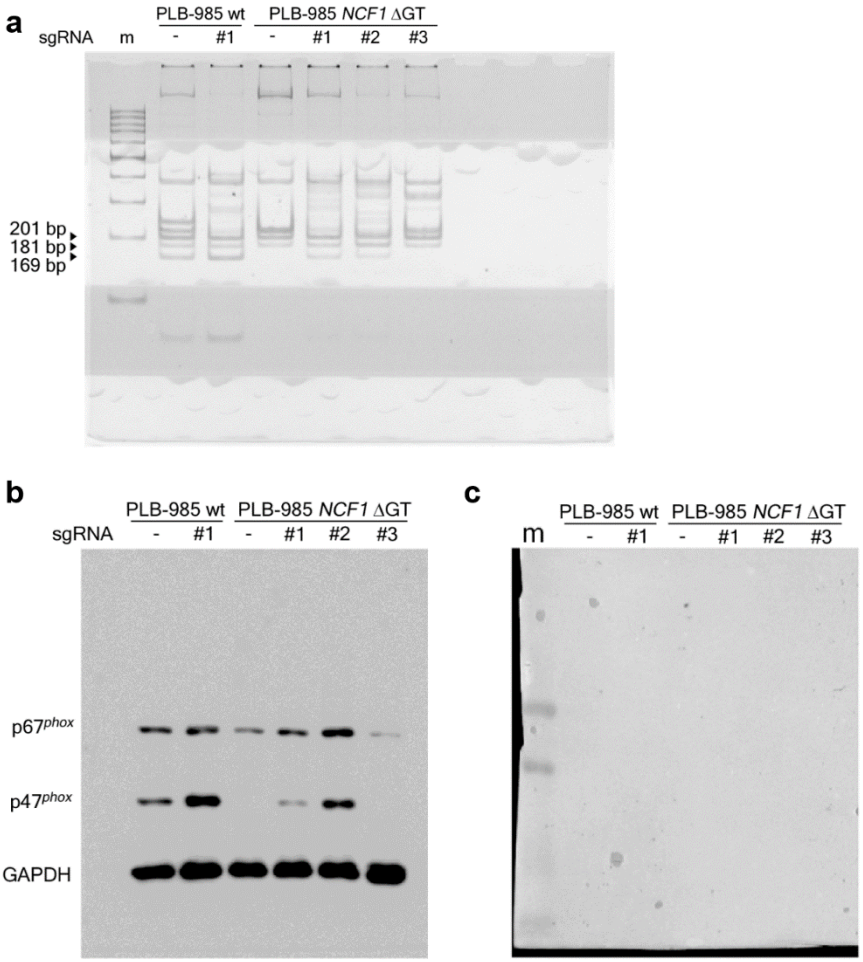

Uncropped and/or unexposed gel and membrane shown in Figure 1 of the main text

(**a**) An image of the uncropped PAGE gel of PCR-RFLP shown in **Figure 1C**.

(**b**) An image of the uncropped western blot membrane displaying expression of p67^{phox} (top), p47^{phox} (middle), and GAPDH (bottom), shown in **Figure 1F**.

(**c**) An image of the unexposed western blot membrane shown in b displays the lane for a protein ladder 'm' (PageRuler™ Plus Prestained Protein Ladder 10 to 250 kDa, Thermo Fisher Scientific).

Supplemental Tables

Table S1

Known genes with disease-causing pseudogenes, co-localized on the same chromosome.[6,11,36-38,50-55]

Gene	Disease	OMIM ID	Genomic location	Coordinates (GRCh38)	Pubmed ID
ABCC6	Pseudoxanthoma elasticum (PXE)	603234	16p13.11	16:16,149,564-16,223,616	11474653
CRYBB2	Autosomal dominant cataract	123620	22q11.23	22:25,211,659-25,231,868	3436525
CYP21A2	Congenital adrenal hyperplasia	613815	6p21.33	6:32,038,315-32,041,669	3486422
FOLR1	Neural tube defects	136430	11q13.4	11:72,189,557-72,196,322	1717147
GBA	Type 2 Gaucher disease	606463	1q22	1:155,234,447-155,244,861	2914709
IDS	Hunter syndrome	300823	Xq28	X:149,476,989-149,505,353	7633410
IGLL1	B cell deficiency and agammaglobulinemia	146770	22q11.23	22:23,573,124-23,580,547	12384776
NCF1	Chronic granulomatous disease	608512	7q11.23	7:74,773,961-74,789,375	9329953
PKD1	Autosomal dominant polycystic kidney disease	601313	16p13.3	16:2,088,707-2,135,897	11414761
SBDS	Shwachman-Bodian-Diamond syndrome	607444	7q11.21	7:66,987,676-66,995,695	12496757
RP9	Autosomal dominant retinitis pigmentosa	607331	7p14.3	7:33,094,796-33,109,389	16671097

Table S2

Potential off-target sites predicted by COSMID Off-Target Analysis Tool.[49]

	Off-target sequence	Mismatch	Cut site	Score	Gene	Primer Forward	Primer Reverse	PCR [bp]	Position
sgRNA#1	TTCACCAGGAACATGTACCTNGG	-	-	-	-	-	-	-	-
1	**G**TCACCA**A**GAACATGTAC**A**TGGG	3	76852825	5.39	*ZFHX4*	AGTGAGTGCAGACTGCCAAA	AAGCTTGTCATAGGCCTCCC	454	Chr8:76852444-76852897
2	T**CA**ACCAGGAACATGTA**A**CTTGG	3	19965860	4.28	*LPL*	TAAGGCTCCTTCATGTGGCG	CCAGGAACCTCTCCACCCTT	766	Chr8:19965618-19966383
3	T**C**CACCA**CT**AACATGTACCTAGG	3	120164679	0.75	*SEC22B*	GCACCCAGCCTATTAGCCGT	ACCCAGCAAACCCATTAATGGGT	929	Chr1:120163868-120164796
4	T**C**CACCAGGA**G**CATGT**T**CCTGGG	3	30276197	3.83	*AL021921.1*	GACAGCCAGACATGGATAACCG	GCCACGCAGTGAGTAAGCTG	828	Chr1:30276795-30275968
5	TTC**T**CCA**T**GAACATGT**T**CCTTGG	3	129559878	3.44	*TMEM132D*	GCTTGGTGCCCACCTATGAA	CACAAATGGGAAGACGCTGG	686	Chr12:129560157-129559472
6	TTC**T**CCAGG**GG**CATGTACCTAGG	3	102323741	1.37	*ZNF839*	ACTCGGGATCACTACTGGCA	TCTCCTGCAACTTGAAAGGGC	740	Chr14:102323227-102323966
7	TTCA**T**CAGGA**T**CATGT**T**CCTAGG	3	15897717	3.89	*LOC102724957*	CAGACAAGGCAGGAGGCAG	CTCCAGCAGTCAAGATCTAGCAC	731	Chr11:15898188-15897458
8	TTCAC**A**AGGA**T**CATGTA**T**CTAGG	3	41091359	4.91	*CNTN1*	CATAGTGGCCTGAAGGCAGTAT	TGGCACTTGAGACACTATTGATCC	769	Chr12:41091848-41091080
9	TTCACC**T**G**T**AACATG**G**ACCTGGG	3	4084965	2.88	*C1orf174*	GAAGAGCAGAGTGGAGGCTC	AGCTGTCTGTCGCACTGGAC	1017	Chr1:4084575-4085591
10	TTCACCAG**CT**ACATGTACCTGGG	2	14512241	0.85	*NFIB*	GGCTAGCCTGAGATGACACAG	GAGAAAAGAAAGACGGGAGGTAGG	1204	Chr9:14511591-14512794
11	TTCACCAGG**GG**CATGT**C**CCTGGG	3	139751840	4.20	*NXPH2*	CAGTCCTGGGGCAAGAACA	CTAGGCTGGATACAGTGACTGC	493	Chr2:139751463-139751955

Table S3

Off-target sites detected by GUIDE-seq.[24] The shaded entries represent one off-target sequence repeated five times in the reference genome.

	Off-target sequence	Position	Strand	Mismatch	Reads	Gene or nearest genes
sgRNA#1	TTCACCAGGAACATGTACCTNGG	-	+/-	-	230959	-
1	TT**TC**CCAGGAACATGTAC**A**TGGG	Chr14:18601333-18601355	-	3		*OR11H12*
2	TT**TC**CCAGGAACATGTAC**A**TGGG	Chr14:19713678-19713700	+	3		*OR11H2*
3	TT**TC**CCAGGAACATGTAC**A**TGGG	Chr15:21574969-21574991	+	3	1750	*POTEB3; OR4N4*
4	TT**TC**CCAGGAACATGTAC**A**TGGG	Chr15:22010291-22010313	+	3		*POTEB; OR4M2*
5	TT**TC**CCAGGAACATGTAC**A**TGGG	Chr22:15528375-15528397	-	3		*OR11H1*
6	T**CTC**CCAGGAACATGTAC**A**TGGG	Chr14:19180507-19180529	-	4	967	*POTEM; POTEG*
7	T**C**C**C**CCAGG**C**A**GG**TG**G**AC**AG**GGG	Chr14:104687804-104687826	+	8	2	*TMEM179; INF2*

Table S4
A list of indel mutations at the CRISPR-Cas9 on-target cleavage site identified by SMRT sequencing within CRISPR-Cas9-treated PLB-985 *NCF1* ΔGT cells (sgRNA #1).

Reference sequences (*NCF1: GTGT*; mutated *NCF1*, *NCF1B*, *NCF1C*: ΔGT)	
GGTCCCCCGACTCTGGCTTTCCCCCAGGTGTACATGTTCCTGGTGAAATGGCAGGACCTGTCGGAG	GTGT
GGTCCCCCGACTCTGGCTTTCCCCCAGGT--ACATGTTCCTGGTGAAATGGCAGGACCTGTCGGAG	ΔGT
Identified indels	SMRT reads [%]
GGTCCCCCGACTCTGGCTTTCCCCCAGG---ACATGTTCCTGGTGAAATGGCAGGACCTGTCGGAG	16.4
GGTCCCCCGACTCTGGCTTTCCCCCAGGT-TACATGTTCCTGGTGAAATGGCAGGACCTGTCGGAG	8.6
GGTCCCCCGACTCTGGCTTTCCCCCA----TACATGTTCCTGGTGAAATGGCAGGACCTGTCGGAG	7.1
GGTCCCCCGACTCTGGCTTTCCCCCAGGTG---------------AAATGGCAGGACCTGTCGGAG	5.3
GGTCCCCCGACTCTGGCTTTCCCCCAGG-------------GGTGAAATGGCAGGACCTGTCGGAG	4.5
GGTCCCCCGACTCTGGCTTTCCCCCAGGT--------TCCTGGTGAAATGGCAGGACCTGTCGGAG	4.7
GGTCCCCCGACTCTGGCTTAC------------ATGTTCCTGGTGAAATGGCAGGACCTGTCGGAG	3.8
GGTCCCCCGACTCTGGCTTTCCCCCA--------TGTTCCTGGTGAAATGGCAGGACCTGTCGGAG	2.5
GGTCCCCCGACTCTGGCTTTCCCCCAGGT---------CCTGGTGAAATGGCAGGACCTGTCGGAG	1.6
GGTCCCCCGACTCTGGCTTTCCCCCAGGGAGGTGTACATGTTCCTGGTGAAATGGCAGGACCTGTCGGAG	1.4
GGTCCCCCGACTCTGGCTTTCCCCCAG---TACATGTTCCTGGTGAAATGGCAGGACCTGTCGGAG	1.4
GGTCCCCCGACTCTGGCTTTCCCCCAGGTTGTACATGTTCCTGGTGAAATGGCAGGACCTGTCGGAG	1.4
GGTCCCCCGACTCTGGCTTTCCCCCAGGT----ATGTTCCTGGTGAAATGGCAGGACCTGTCGGAG	1.4
GGTCCCCCGACTCTGGCTTTCCCCCAGGT------------GGTGAAATGGCAGGACCTGTCGGAG	1.2
GGTCCCCCGACTCTGGCTTTCCCCCAGGTTTGTACATGTTCCTGGTGAAATGGCAGGACCTGTCGGAG	1.2
GGTCCCCCGACTCTGGCTTTCCCCCAGG----CATGTTCCTGGTGAAATGGCAGGACCTGTCGGAG	1.0
GGTCCCCCGACTCTGGCTTTCCCCCAGG--------------GTGAAATGGCAGGACCTGTCGGAG	1.0
GGTCCCCCGACTCTGGCTTTCCCCCAG-T-TACATGTTCCTGGTGAAATGGCAGGACCTGTCGGAG	0.9
GGTCCCCCGACTCTGG---------------------------TGAAATGGCAGGACCTGTCGGAG	0.8
GGTCCCCCGACTCTGGCTTTCCCCCAG----ACATGTTCCTGGTGAAATGGCAGGACCTGTCGGAG	0.8
GGTCCCCCGACTCTGGCTTTCCCCCAGGGGTACATGTTCCTGGTGAAATGGCAGGACCTGTCGGAG	0.7
GGTCCCCCGACTCTGGCTTTCCCCCAGGGTGTACATGTTCCTGGTGAAATGGCAGGACCTGTCGGAG	0.7
GGTCCCCCGACTCTGGCTTTCCCCCAGG-GTACATGTTCCTGGTGAAATGGCAGGACCTGTCGGAG	0.7
GGTCCCCCGACTCTGGCTTTCCCCCAGG-------GTTCCTGGTGAAATGGCAGGACCTGTCGGAG	0.7
GGTCCCCCGACTCTGGCTTTCCCCCAGGGGTGTACATGTTCCTGGTGAAATGGCAGGACCTGTCGGAG	0.6
GGTCCCCCGACTCTGGCTTTCCCCCAGGT-------TTCCTGGTGAAATGGCAGGACCTGTCGGAG	0.6
GGTCCCCCGACTCTGGCTTTCC------------TGTTCCTGGTGAAATGGCAGGACCTGTCGGAG	0.5
GGTCCCCCGACTCTGGCTTTCCCCCAGG----------CCTGGTGAAATGGCAGGACCTGTCGGAG	0.5
GGTCCCCCGACTCTGGCTTTCCCCCA--------TGT-CCTGGTGAAATGGCAGGACCTGTCGGAG	0.5
GGTCCCCCGACTCTGGCTTT----------TACATGTTCCTGGTGAAATGGCAGGACCTGTCGGAG	0.5
GGTCCCCCGACTCTGGCTTTCCCCC---TG--CATGTTCCTGGTGAAATGGCAGGACCTGTCGGAG	0.4
GGTCCCCCGACTCTGGCTTTCCCCCAGG----------------GGAATGGCAGGACCTGTCGGAG	0.3
GGTCCCCCGACTCTGGCTTTCCCCCAGG-G-ACATGTTCCTGGTGAAATGGCAGGACCTGTCGGAG	0.3
GGTCCCCCGACTCTGGCTTTCCCCCAGG-G-------TCCTGGTGAAATGGCAGGACCTGTCGGAG	0.3
GGTCCCCCGACTCTGGCTTTCCCCCAGG-----ATGTT---GGTGAAATGGCAGGACCTGTCGGAG	0.3
GGTCCCCCGACTCTGGCTTTCCCCCAGGTGT------TCCTGGTGAAATGGCAGGACCTGTCGGAG	0.3
GGTCCCCCGACTCTGGCTTTCCCCCA--------TGTT---GGTGAAATGGCAGGACCTGTCGGAG	0.3

GGTCCCCCGACTCTGGCTTTCCCCCAGG-----ATGTTC-TGGTGAAATGGCAGGACCTGTCGGAG	0.3
GGTCCCCCGACTCTGGCTTTCCCCCAGG----------AAATGGCAGGACCTGTCGGAG	0.3
GGTCCCCCGACTCTGGCTTTCCC--------ACATGTTCCTGGTGAAATGGCAGGACCTGTCGGAG	0.3
GGTCCCCCGACTCTGGCTTTCCCCCAGGT-TACATGTTCCTGGTGAAATGGCAGGACCTGTCGGAG	0.3
GGTCCCCCGACTCTGGCTTTCCCC---------ATGTTCCTGGTGAAATGGCAGGACCTGTCGGAG	0.2
GGTCCCCCGACTCTGGCTTCCCC--AGGT--ACATGTTCCTGGTGAAATGGCAGGACCTGTCGGAG	0.2
GGTCCCCCGACTCTGGCTTTCCCCCAGGGGGTACATGTTCCTGGTGAAATGGCAGGACCTGTCGGAG	0.2
GGTCCCCCGACTCTGGCTTTCCCC-------ACATGTTCCTGGTGAAATGGCAGGACCTGTCGGAG	0.2
GGTCCCCCGACTCTGGCTTTCCCCCAGGT--ACA--TTCCTGGTGAAATGGCAGGACCTGTCGGAG	0.2

Table S5

Primers used for the assessment of CNV by qPCR (**Figure2A and Figure 2B**).

Gene	**Location relative to *NCF1* loci**	**Forward primer**	**Reverse primer**
CALN1	Centromeric side of *NCF1B*	GGTGATTGGCTGTGTCTTCC	CCGGCTAAGTAATCAGCTCCA
EIF4H	Between *NCF1B* and *NCF1*	TCAGAAAAGGTGGACCAGATGAC	GGAACGTTCACGAGTTGGAAT
WBSCR16	Between *NCF1* and *NCF1C*	CCTGGGATTCCATCTGGAGC	CGATTCTCTTCCTGAGGGGC
HIP1	Telomeric side of *NCF1*	GAAGCCTTGCCTCCTCAACT	GGTCTGGTTGGAGATGGGTG
SOD1	Chromosome 21 (reference)	CAGAGGCCTTGGGACATAGC	ATGGGGCTGCACCTGATTTC

Table S6
Chromosomal aberrations identified for the PLB-985 *NCF1* ΔGT cell line.

	Chromosome	Locus	Start	End	Size [kb]	Mean log2 ratio	Median log2 ratio	Copy number
1	1	q21.1:q23.2	145382123	159863470	14481.3	0.2790	0.2892	3
2	3	p21.31	45599905	47567580	1967.7	0.3130	0.3204	3
3	3	p21.31	47570543	47654374	83.8	-0.5346	-0.5187	1
4	4	p15.1	34779031	34824169	45.1	-2.0251	-2.0282	0
5	4	q28.3	135061532	135094781	33.2	-0.5964	-0.5888	1
6	4	q35.1:q35.2	186676232	188997015	2320.8	-0.6406	-0.6358	1
7	5	q11.2:q.23.3	53675286	127682183	74006.9	-0.5359	-0.5318	1
8	5	q23.3:q31.1	128172849	135619529	7446.7	-0.5231	-0.5175	1
9	5	q31.1:q31.3	135842660	139578983	3736.3	-0.5387	-0.5366	1
10	5	q33.3	156811544	156903327	91.8	-0.5009	-0.5014	1
11	6	q13	74590396	74601723	11.3	-1.5305	-1.5288	0
12	6	q26	162722580	162912831	190.3	0.3081	0.3003	3
13	7	q32.2	130810971	131005889	194.9	-0.5437	-0.5412	1
14	8	q24.13	126224383	126547568	323.2	1.1117	1.1269	4
15	8	q24.13:q24.21	126712969	127390069	677.1	1.1220	1.1502	4
16	8	q24.21	128075476	128345268	269.8	1.1384	1.1348	4
17	8	q24.21	128690529	128771759	81.2	1.2554	1.2835	4
18	8	q24.21	129987555	130209520	222.0	1.4051	1.4172	4
19	8	q24.21	130366403	130697499	331.1	1.4732	1.4976	4
20	9	p23:p21.1	11774820	32397138	20622.3	-0.5663	-0.5651	1
21	9	q31.1	104636449	106946358	2309.9	-0.6005	-0.5927	1
22	10	p15.3:p12.1	100026	25425701	25325.7	-0.5498	-0.5464	1
23	13	q11:q12.12	19436286	23397468	3961.2	-0.5003	-0.5002	1
24	14	q23.2	62173186	62630023	456.8	-0.5433	-0.5439	1
25	14	q23.2:q31.1	64716201	81909742	17193.5	-0.5285	-0.5254	1
26	14	q32.33	106329183	106723341	394.2	0.3315	0.3058	3
27	15	q11.2:q15.3	22770421	43976996	21206.6	-0.5398	-0.5348	1
28	16	q23.2:q23.3	81280004	81897623	617.6	-0.5104	-0.5030	1
29	16	q24.1:q24.3	85510923	90146767	4635.8	-0.5154	-0.5048	1
30	17	p13.3:p11.2	525	17099612	17099.1	-0.5364	-0.5257	1
31	17	p11.2	18144526	20753871	2609.3	-0.5252	-0.5234	1
32	17	q12	36350597	36404135	53.5	-0.5300	0.5234	1
33	18	trisomy				0.3026	0.3080	
34	19	p12	20598429	20720704	122.3	-0.486	-0.447	1
35	22	q11.23:q12.1	25656237	25922333	266.1	0.4080	0.4057	3
36	X	monosomy				-0.5191	-0.5161	

Table S7
De novo chromosomal aberrations identified for selected clones of CRISPR-Cas9-treated PLB-985 *NCF1* ΔGT cell line by aCGH.

clone 1								
	Chromosome	Locus	Start	End	Size [kb]	Mean log2 ratio	Median log2 ratio	Copy number
1	9	p21.1:q31.1	32406181	104628430	72222.2	0.3072	0.3126	3
2	10	p14	9668766	11590968	1922.2	-2.0910	-2.0904	0
3	13	q21.2	61021403	61040152	18.7	-0.4828	-0.5300	1
4	14	p23.2	62634687	64690561	2055.9	0.2617	0.2653	3
5	14	q31.1:q32.33	81923332	107145067	25221.7	0.3092	0.3146	3
clone 21 No aberrations								
clone 22								
	Chromosome	Locus	Start	End	Size [kb]	Mean log2 ratio	Median log2 ratio	Copy number
1	1	p34.3	35771294	35783945	12.7	-0.5677	-0.5505	1
clone 27								
	Chromosome	Locus	Start	End	Size [kb]	Mean log2 ratio	Median log2 ratio	Copy number
1	10	q22.1	70692429	70932814	240.4	0.318	0.327	3
clone 32								
	Chromosome	Locus	Start	End	Size [kb]	Mean log2 ratio	Median log2 ratio	Copy number
1	6	trisomy				0.2926	0.2980	3
2	7	q11.23	72636883	74141745	1504.9	-0.4664	-0.4736	1
3	7	q11.23	74191290	74578927	387.6	-0.4610	-0.4654	1
4	9	p21.1:q31.1	32406181	104628430	72222.2	0.2918	0.2968	3
5	14	q23.2	62634525	64686542	2052.0	0.2431	0.2469	3
6	14	q31.1:q32.33	81923332	107145067	25221.7	0.2956	0.2999	3
clone 39 No aberrations								
clone 40								
	Chromosome	Locus	Start	End	Size [kb]	Mean log2 ratio	Median log2 ratio	Copy number
1	7	q11.23	74197396	74578927	381,5	-0.332	-0.337	1
clone 41								
	Chromosome	Locus	Start	End	Size [kb]	Mean log2 ratio	Median log2 ratio	Copy number
1	7	q11.23	74191290	74286808	95.5	-0.384	-0.365	1
2	7	q11.23	74404149	74578928	174.8	-0.424	-0.415	1
clone 48								
	Chromosome	Locus	Start	End	Size [kb]	Mean log2 ratio	Median log2 ratio	Copy number
1	6	trisomy				0.2732	0.2778	3

2	7	q11.23	72637752	74141492	1503.7	-0.4462	-0.4467	1
3	7	q11.23	74190888	74578927	388.0	-0.4162	-0.4404	1
4	9	p21.1:q31.1	32409908	104622867	72213.0	0.2809	0.2837	3
5	14	q23.2	62634753	64704354	2069.6	0.2251	0.2311	3
6	14	q31.1:q32.33	81939428	107145067	25205.6	0.2830	0.2875	3
clone 49								
	Chromosome	Locus	Start	End	Size [kb]	Mean log2 ratio	Median log2 ratio	Copy number
1	6	p21.33	31566126	31757782	191.7	0.300	0.283	3
2	7	q11.23	72637752	74578927	1941.2	-0.430	-0.436	1

Supplemental references

45. Wohlgensinger, V., Seger, R., Ryan, M. D., Reichenbach, J. & Siler, U. Signed outside: A surface marker system for transgenic cytoplasmic proteins. *Gene Ther.* **17**, 1193–1199 (2010).
46. Jinek, M. *et al.* A programmable dual-RNA-guided DNA endonuclease in adaptive bacterial immunity. *Science* **337**, 816–21 (2012).
47. Pedruzzi, E., Fay, M., Elbim, C., Gaudry, M. & Gougerot-Pocidalo, M.-A. Differentiation of PLB-985 myeloid cells into mature neutrophils, shown by degranulation of terminally differentiated compartments in response to N-formyl peptide and priming of superoxide anion production by granulocyte-macrophage colony-stimulating fact. *Br. J. Haematol.* **117**, 719–26 (2002).
48. Drexler, H. G., Dirks, W. G., Matsuo, Y. & MacLeod, R. A. F. False leukemia-lymphoma cell lines: An update on over 500 cell lines. *Leukemia* **17**, 416–426 (2003).
49. Cradick, T. J., Qiu, P., Lee, C. M., Fine, E. J. & Bao, G. COSMID: A web-based tool for identifying and validating CRISPR/Cas off-target sites. *Mol. Ther. - Nucleic Acids* **3**, e214 (2014).
50. Germain, D. P. Pseudoxanthoma elasticum: evidence for the existence of a pseudogene highly homologous to the ABCC6 gene. *J. Med. Genet.* **38**, 457–61 (2001).
51. Aarts, H. J., Den Dunnen, J. T., Lubsen, N. H. & Schoenmakers, J. G. Linkage between the beta B2 and beta B3 crystallin genes in man and rat: a remnant of an ancient beta-crystallin gene cluster. *Gene* **59**, 127–35 (1987).
52. Higashi, Y., Yoshioka, H., Yamane, M., Gotoh, O. & Fujii-Kuriyama, Y. Complete nucleotide sequence of two steroid 21-hydroxylase genes tandemly arranged in human chromosome: a pseudogene and a genuine gene. *Proc. Natl. Acad. Sci. U. S. A.* **83**, 2841–2845 (1986).
53. Bondeson, M. L. *et al.* Inversion of the IDS gene resulting from recombination with IDS-related sequences in a common cause of the hunter syndrome. *Hum. Mol. Genet.* **4**, 615–621 (1995).
54. Linnebank, M. *et al.* Argininosuccinate lyase (ASL) deficiency: mutation analysis in 27 patients and a completed structure of the human ASL gene. *Hum. Genet.* **111**, 350–9 (2002).
55. Boocock, G. R. B. *et al.* Mutations in SBDS are associated with Shwachman-Diamond syndrome. *Nat. Genet.* **33**, 97–101 (2003).